"More is Different": Synergistic Effect and Structural Engineering in Double-Atom Catalysts

Yiran Ying, Xin Luo, Jinli Qiao, and Haitao Huang*

Yiran Ying and Prof. Haitao Huang

Department of Applied Physics and Research Institute for Smart Energy, The Hong Kong Polytechnic University, Hung Hom, Kowloon, Hong Kong

*Email: aphhuang@polyu.edu.hk

Prof. Xin Luo

State Key Laboratory of Optoelectronic Materials and Technologies, Centre for Physical Mechanics and Biophysics, School of Physics, Sun Yat-sen University, Guangzhou, P.R. China, 510275

Prof. Jinli Qiao

State Key Laboratory for Modification of Chemical Fibers and Polymer Materials, College of Environmental Science and Engineering, Donghua University, 2999 Renmin North Road, Shanghai 201620, P. R. China.

Abstract. Double-atom catalysts (DACs) have emerged as a novel frontier in heterogeneous catalysis because the synergistic effect between adjacent active sites can promote their catalytic activity while maintaining high atomic utilization efficiency, good selectivity, and high stability originating from the atomically dispersed nature. In this review, we focus on the recent progress in both experimental and theoretical research on DACs for various catalytic reactions. Specifically, the central tasks in the design of DACs—manipulating the synergistic effect and engineering atomic and electronic structures of catalysts—are systematically reviewed, along with the prevailing experimental, characterization, and computational modeling approaches. Furthermore, we address the practical applications of DACs in water splitting, oxygen reduction reaction, nitrogen reduction reaction, and carbon dioxide reduction reaction. Finally, we summarize the future challenges for DACs and provide an outlook on the further investigations of DACs toward heterogeneous catalysis in high-performance energy and environmental applications.

1. Introduction

With the rapid development of industrialization, energy and environment have become crucial issues for human beings.[1] Fossil fuels, including coal, petroleum, and natural gas, have been the most predominant energy sources globally, accounting for approximately 85% of the world's energy consumption in 2018.[2] However, the non-renewable nature of fossil fuels has raised a global concern regarding their depletion, considering the accelerating consumption per year owing to the global economic boost and population growth. To make things worse, fossil fuels raise environmental concerns such as greenhouse gas emissions and global warming.[1, 3] Consequently, there is an urgent need for developing sustainable and renewable energy sources and constructing large-scale infrastructure for practical applications in order to solve the energy crisis and reduce environmental pollution.

Heterogeneous catalysis, which can expedite chemical reactions on electrochemical interfaces,[4] plays a significant role in energy conversion processes and thus has gained increasing attention. Compared with homogeneous catalysts, heterogeneous catalysts can endure harsh reaction conditions and can be conveniently separated from the reaction systems and thus are more widely applied in practical applications.[5] The most consistently studied heterogeneous catalytic reactions for energy and environmental applications include hydrogen evolution reaction (HER),[6] oxygen evolution reaction (OER),[6b, 6e, 7] oxygen reduction reaction (ORR),[6e, 8] nitrogen reduction reaction (NRR),[9] and CO_2 reduction reaction (CO_2RR)[10]. Water splitting via HER and OER can facilitate the production of hydrogen, a clean energy carrier with high mass density, which can be a promising substitute for fossil fuels. ORR is the bottleneck reaction for proton-exchange membrane fuel cells, and the performance enhancement of ORR can benefit the efficient and environmentally friendly energy conversion in the fuel cells. NRR is the less energy-consuming

approach for converting dinitrogen (N_2) to ammonia (NH_3), an important chemical used in the industry and agriculture, as well as an efficient energy carrier. CO_2RR shows significance in the carbon cycle, achieving the reduction of CO_2 in the environment and production of value-added chemicals simultaneously. The most important task in heterogeneous catalysis is the design of highly efficient catalysts in overcoming the kinetic energy barrier in practical catalytic reactions. However, the high cost and natural scarcity of conventional noble metal and metal oxide catalysts hinder their industrial applications. On the other hand, single-atom catalysts (SACs), since the first report of Pt_1/FeO_x catalyst for CO oxidation in 2011,[11] have attracted widespread attention because of their high atom utilization efficiencies (AUEs), close to 100%, outstanding selectivity, and high stability.[5, 12] SACs can form a bridge between heterogeneous and homogeneous catalysts by introducing the advantages of homogeneous catalysis—high selectivity—into heterogeneous catalysis by uniform and controllable atomically dispersed active sites.[13] Much progress has been made in SACs in the past decade, with multiple applications in water splitting,[14] ORR,[15] NRR,[16] and CO_2RR[17]. Despite the broad prospect of single-atom catalysis, SACs suffer from structural simplicity and lack of synergistic active sites for surpassing the intrinsic performance limit of more complicated electrocatalytic reactions, which include multiple reaction steps and reaction intermediates, such as ORR, CO_2RR, and NRR.[5, 18]

A promising approach to solving this issue is the introduction of dual active sites, forming dimers supported on substrates, which are known as double-atom catalysts (DACs), or dual-atom catalysts, instead of SACs (**Figure 1**).[5, 18-19] In 2014, He *et al.* reported the controlled synthesis of Fe dimers incorporated into a graphene lattice by drop-casting a solution of $FeCl_3$ onto clean graphene samples,[20] inspiring research into introducing metal dimers supported on vacancies or defect sites of materials to form metal dimers, which have potential applications in heterogeneous

catalysis. In his famous article 'More is Different', P.W. Anderson stated that 'at each level of complexity entirely new properties appear'.[21] DACs are more than simple doubling of single atom and they may introduce a synergistic effect to break the theoretical limit of SACs.[18-19, 22] However, owing to significant issues such as the difficulty of precise control of metal dimers, obstacles exist in the experimental studies of DACs. To overcome these challenges, experimentalists seek solutions by renovating and establishing novel synthesis methods for the precise control of the atomic structures of DACs, while theoretical chemists aim to develop tools for the computational design and prediction of potential DACs with high performance and provide guidance to experimentalists by proposing and analyzing the catalytic mechanisms. They go through two different expeditions with the same ultimate goal: fully utilizing the synergistic effect in DACs by structural engineering to obtain better catalysts (**Figure 1**).
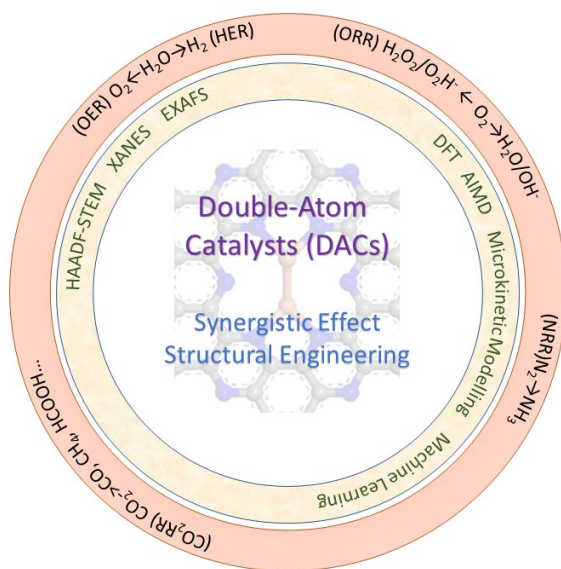

Figure 1. Schematic of experimental and theoretical techniques used in recent investigations for the advancement of DACs.

The above-mentioned prospects and challenges in the design of DACs make it one of the most intriguing topics in electrocatalysis and photocatalysis. In this review, we first comprehensively summarize the experimental and theoretical methodologies in the preparation, characterization, and prediction of DACs for various energy-related catalytic applications, including water splitting, ORR, NRR, and CO_2RR. Then, the current progress is systematically reviewed based on different reactions, with a focus on the role of the nature of the dual-atom in the improvement of catalytic activities. Finally, we point out the challenges in DACs and provide an outlook on this emerging area.

2. Preparation and Characterization Methods for DACs

2.1 Preparation of DACs

The most important prerequisite for research in laboratories and practical applications of DACs is the chemical synthesis of metal dimers that can be stably anchored on substrates. Since the surface free energy of metal atoms is higher than that of nanoparticles, similar to SACs, one major challenge to stabilize DACs is preventing the aggregation of isolated metal atoms during synthesis and catalytic reactions.[12a] To achieve this, strong covalent bonds between the metal dimers and the coordinated atoms are crucial to lower the free energy of metal dimers or increase the aggregation energy barrier. Multiple attempts to stabilize SACs have resulted in successful synthesis, with methods including spatial confinement, coordination site construction, chemical etching, defect design, and electro-/photochemical strategies.[23] Nevertheless, the synthesis of DACs is more challenging owing to the complexity of precise control of metal dimers, and thus, there is an urgent need to develop a more precise design of the structural engineering approach.

Thus, in this section, we review the current strategies used for the synthesis of DACs, which are categorized into bottom-up and top-down strategies.

2.1.1 Bottom-up Strategies

For bottom-up strategies, mono- or multi-nucleus metal complex precursors are first adsorbed and finally reduced and confined in vacancies to form DACs.[23] Atomic layer deposition (ALD), with a sequence of self-limiting reactions in which metal, metal oxides, or other materials can be uniformly deposited on the surface, results in the precise control of metal particle size, composition, and structure.[24] The uniform deposition character of ALD makes it a powerful approach for the construction of atomic catalysts and investigation of structure-performance relations, particularly for the precise fabrication of DACs.[25] Yan *et al.* reported the synthesis of Pt_2 dimers on graphene (**Figure 2a**) using the bottom-up ALD technique.[25a] First, isolated anchoring sites for DACs on graphene were created by acid oxidation and high-temperature thermal reduction; then, the first cycle of Pt ALD was performed by exposing trimethyl(methylcyclopentadienyl)-platinum (IV) ($MeCpPtMe_3$) and molecular O_2 at 250 °C to form Pt_1@graphene, followed by the second ALD cycle, in which secondary Pt atoms are deposited on the preliminary ones at a lower temperature of 150 °C to prevent metal atom aggregation. Finally, Pt_2@graphene DACs were fabricated. The as-synthesized DACs exhibited a high specific rate of 2800 mol_{H2} mol_{Pt}^{-1} min^{-1} at room temperature in the hydrolytic dehydrogenation of ammonia borane, which was approximately 17- and 45-fold higher than that of Pt SACs and nanoparticles. Heteronuclear DACs Pt-Ru dimers supported on nitrogen-doped carbon nanotubes (NCNTs) can also be prepared using ALD (**Figure 2b**).[25b] Owing to the difficulty in depositing Ru on NCNTs in the first few ALD cycles, the authors first prepared Pt

SACs with MeCpPtMe$_3$ precursors. In the second round of ALD, Ru(C$_2$H$_5$C$_5$H$_4$)$_2$ was selected as the precursor to selectively deposit Ru on Pt single-atoms to form Pt-Ru DACs.
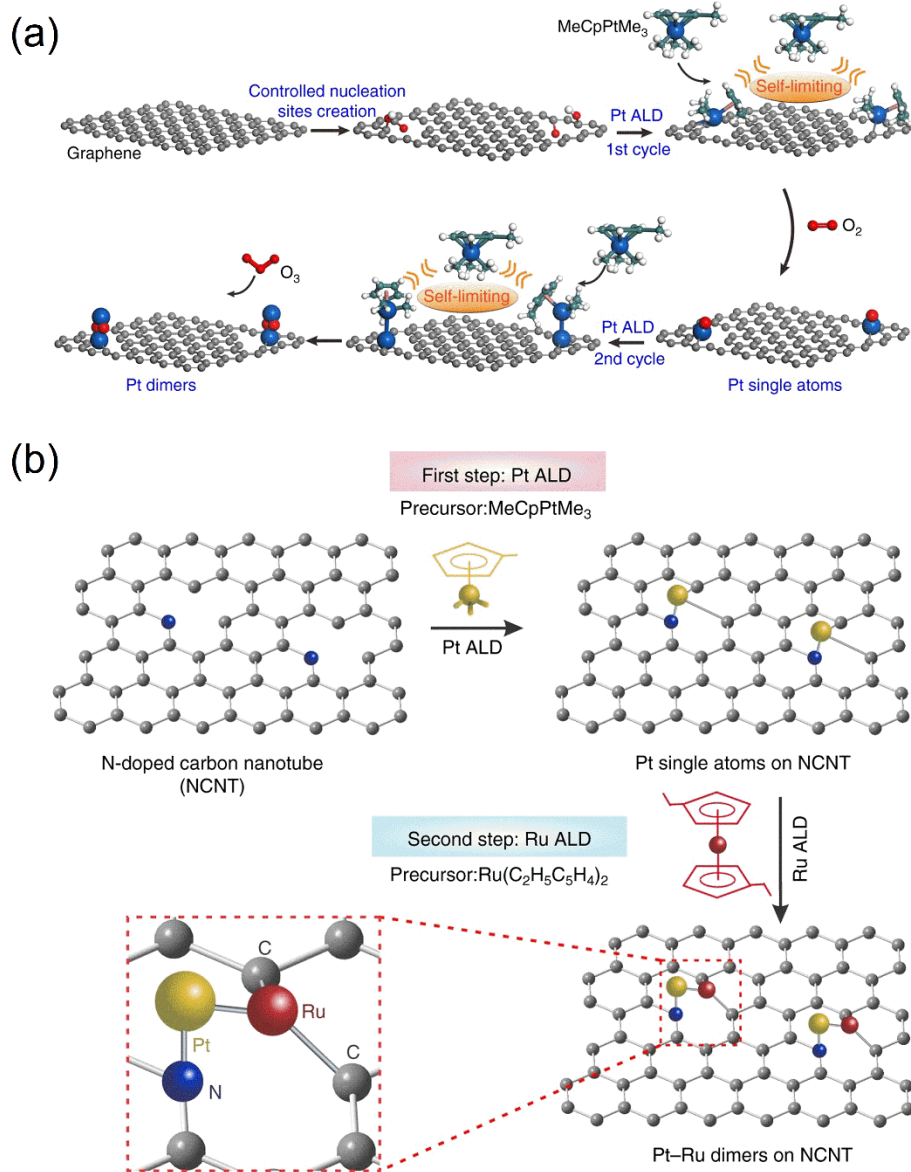

Figure 2. Schematic of bottom-up synthesis of DACs by ALD. (a) Synthesis of Pt$_2$/graphene (carbon in cyan; hydrogen in white; oxygen in red; and platinum in blue) Reproduced with

permission.[25a] Copyright 2017, Nature Publishing Group. (b) Synthesis of Pt-Ru dimers on NCNTs. Reproduced with permission.[25b] Copyright 2019, Nature Publishing Group.

Another bottom-up strategy for the synthesis of DACs is the wet-chemistry method, which is considered the simplest and the most promising method for the preparation of SACs.[6e] The electrochemical deposition strategy, as a low-cost and highly efficient method, is widely used in surface modification and is also applicable for the synthesis of DACs, according to the pioneering work by Yao's group.[26] They used a two-step synthesis method with rod-like cobalt-based metal-organic frameworks (MOFs) as precursors. Carbonization at 850 °C with N-doping was performed in the first step and core-shell Co-NC structures were formed. In the second step, by applying cyclic electrochemical potential to Co-NC, carbon-based hollow structures with graphitic shells were formed (**Figure 3**) and Co and Pt were atomically dispersed in NC. The as-fabricated A-CoPt-NC DACs exhibited high activity for ORR (mass activity of 45.47 A mg^{-1})[26a] and HER (overpotential of 27 mV at 10 mA cm^{-2})[26b], which is superior to that of commercial Pt/C catalysts. In addition, another wet-chemistry strategy, the "precursor-preselected" method, was developed by Wang's group to synthesize Fe$_2$ DACs on mesoporous graphitic carbon nitride (mpg-C$_3$N$_4$).[27] The DACs were formed by the preselection of metal precursors and carefully controlled pyrolysis to ensure the double-atom nature and avoid agglomeration; mpg-C$_3$N$_4$ provided anchoring sites for stabilizing DACs. Consequently, the DACs showed excellent performance for alkene epoxidation (*trans*-stilbene → *trans*-stilbene oxide), while the Fe porphyrin, SACs, and nanoparticles were almost inert in reaction.

Figure 3. Schematic of bottom-up synthesis of A-CoPt-NC DACs by electrochemical deposition method. Reproduced with permission.[26b] Copyright 2019, Wiley-VCH Verlag GmbH & Co. KGaA, Weinheim.

2.1.2 Top-down Strategies

For top-down strategies, bulk metal or metal nanoparticles are used as precursors, and DACs are formed by breaking the metal-metal bond to generate atomically dispersed metal dimers on the substrates.[23] To trigger this process, high temperatures are usually used during the synthesis. High-temperature pyrolysis of MOFs containing specific metal atoms is a commonly used approach in the synthesis of DACs anchored on carbon-based materials.[28] Wang *et al.* reported the synthesis of Fe-Co DACs supported on N-doped carbon (N-C) by a host-guest strategy (**Figure 4a**).[28a] They used a bimetallic (Zn/Co) MOF as the host material, and $FeCl_3$ molecules were encapsulated in the cavities. Fe species in the cavities could further expedite the decomposition of the links between metal atoms and the imidazolate structure, forming enlarged voids inside the MOFs. Finally, the Zn species could be removed by volatilization due to its low boiling temperature, and (Fe,Co)/N-C DACs were formed. In another work, Zn-based energetic

MOFs doped with Fe/Co were used as precursors to synthesize CoFe@C DACs by one-step pyrolysis (**Figure 4b**).[28b] During pyrolysis, the Zn nodes were volatilized, and the gases released by the decomposition of energetic triazole ligands induced hierarchically porous carbon networks with Co-Fe double-atoms dispersed on them. In addition, in situ encapsulation of $Fe_2(CO)_9$ in the cavity of zeolitic imidazolate framework (ZIF) before pyrolysis is demonstrated as a feasible approach to provide confinement for the formation of homonuclear Fe_2-based DACs,[28d] while a similar strategy can be extended to triple-atom catalysts by fabricating Ru_3 trimers for catalytic applications.[29]
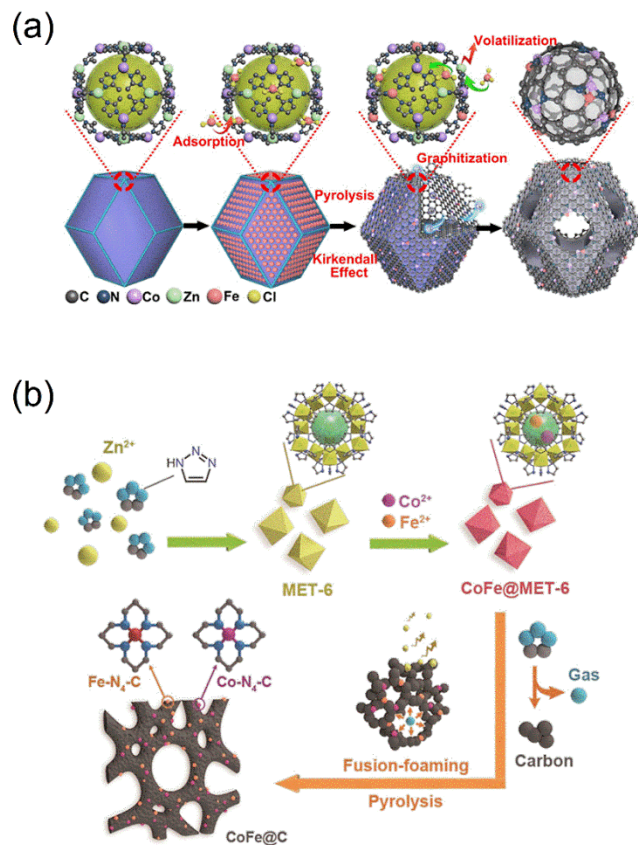
Figure 4. Schematic of top-down synthesis of DACs by high-temperature pyrolysis. (a) Synthesis of (Fe,Co)/N-C. Reproduced with permission.[28a] Copyright 2017, American Chemical Society. (b) Synthesis of CoFe@C. Reproduced with permission.[28b] Copyright 2019, Wiley-VCH Verlag GmbH & Co. KGaA, Weinheim.

2.2 Characterization Methods for DACs

Following the synthesis, the engineered structures in DACs must be investigated using modern characterization methods to confirm the dual-atom structure and explore the intrinsic atomic and electronic structures, as well as the relationship between the structure and the catalytic performance. In this section, we discuss two major characterization methods for DACs: transmission electron microscopy (TEM) and X-ray absorption spectroscopy (XAS).

2.2.1 TEM

TEM is one of the most frequently used techniques in the visualization of the morphology and atomic structures of catalysts.[30] To characterize atomically dispersed active sites, more advanced techniques with better resolution, such as the aberration-corrected high-angle annular dark-field scanning TEM (HAADF-STEM), are indispensable for probing the atomic structures of SACs and DACs.[31] One example shown in **Figure 5** is the application of HAADF-STEM for the characterization of $Ir_2@\alpha\text{-}Fe_2O_3$ DACs.[32] In **Figure 5a and 5b**, the bright two-point structures can be ascribed to Ir_2 DACs, while lighter gray spots in the background represent Fe atoms on the substrate. In addition, few Ir single-atoms or nanoparticle structures can be viewed, confirming the unmixed nature of the as-fabricated DACs. To obtain deeper knowledge, a scan of HAADF

intensity along the dotted line marked in **Figure 5b** was obtained (**Figure 5c**), and the double Ir atoms at a distance of ~3 Å can be clearly seen. Elemental mapping was performed using energy-dispersive X-ray spectroscopy (EDS) incorporated with STEM, and no obvious large aggregation of Ir clusters was observed (**Figure 5d,e**). This work indicates the important role of the advanced TEM technique in the characterization of DACs.
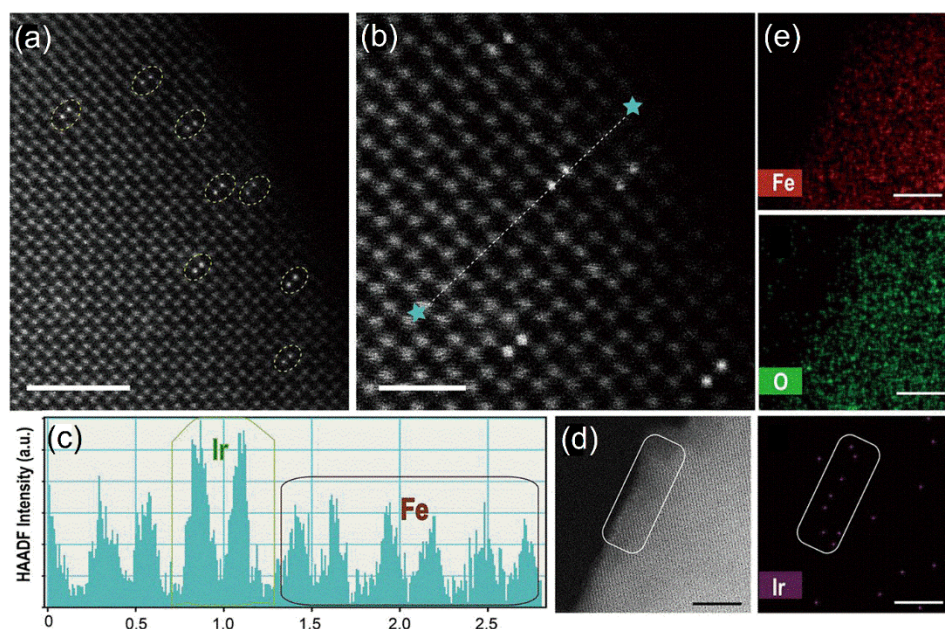
Figure 5. TEM characterization of Ir$_2$ DACs on α-Fe$_2$O$_3$. (a)(b) HAADF-STEM images for Ir$_2$ dimers and (c) the line-scan HAADF intensity analysis results along the line in (b). (d) Dark-field image of the region and (e) the corresponding distribution of Fe, O, and Ir. Scale bar: (a) 2 nm; (b) 1 nm; (d)(e) 4 nm. Reproduced with permission.[32] Copyright 2018, National Academy of Science of the United States of America.

2.2.2 XAS

Synchrotron-radiation X-ray absorption fine structure (XAFS), which can be categorized into X-ray absorption near-edge structure (XANES) and extended X-ray absorption fine structure (EXAFS), is a widely used materials characterization technique to determine the local coordination environment and electronic structure based on XAS.[33] The XAS technique has wide applications in transition metal (TM)-based catalysts because of its element specificity, sensitivity to short-range interaction, and chemical state. Structural information including bond distance, coordination number, oxidation state, and degree of the disorder can be obtained from the analysis of XAS results.[33b, 34] In Wang *et al.*'s work, XANES and EXAFS were applied to study the coordination environment and electronic structure of (Fe,Co)/N-C DACs.[28a] Fe L-edge XANES spectra of (Fe,Co)/N-C showed a single Fe L_3-edge peak, indicating delocalized Fe 3d electrons and high conductivity of the structures (**Figure 6a**). From the N K-edge XAS profiles, peaks corresponding to the π^* and σ^* bands can be observed (**Figure 6b**), and a decrease in the π^* intensity for (Fe,Co)/N-C demonstrated a reduction in the N-C bond length and metal-nitrogen coordination retention after pyrolysis. EXAFS was further applied to reveal the structures of the active sites. The peak at 1.5 Å was ascribed to the Fe–N coordination path for (Fe,Co)/N-C, and the fitting results demonstrated that the coordination numbers for Fe-N and Fe-Co were approximately 3 and 1, respectively (**Figure 6c,d**). Based on these results, a schematic model was built, as shown in **Figure 6e**, and was used in the following theoretical calculations. This work demonstrated that XAFS is of vital importance in the determination of the local coordination environment and atomic structure of DACs.
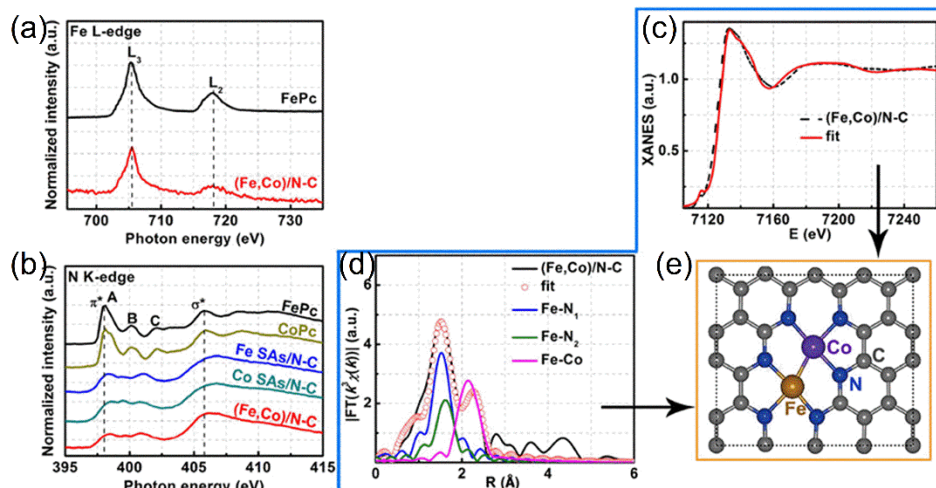
Figure 6. XAS characterization of (Fe,Co)/N-C DACS. (a) Fe L-edge XANES spectra (b) N K-edge XAS profiles of Fe single-atoms (SAs), Co SAs, (Fe,Co)/N-C, (c) K-edge XANES spectra for (Fe,Co)/N-C, and (d) the corresponding Fe K-edge EXAFS fittings, and (e) proposed structures of Fe-Co DACs. Reproduced with permission.[28a] Copyright 2017, American Chemical Society.

3. Exploration of DACs by Theoretical Modeling

For the exploration of electronic structures and reaction mechanisms that underpin the catalytic performance of novel catalysts, theoretical modeling always works in close collaboration with experiments.[35] Because of the multiple possibilities of metal combinations for the formation of DACs as well as the difficulties in precisely controlling the synthesis of atomically dispersed metal dimers, trial-and-error experiments with high economic and time costs are not suitable for large-scale DAC prediction. Therefore, theoretical modeling approaches, including density functional theory (DFT) calculations, ab initio molecular dynamics (AIMD) simulations, microkinetic modeling, and machine learning (ML), play a pivotal role in the design and mechanism of DACs, as well as in explaining experimental phenomena (**Figure 7**). The

importance of theoretical modeling in DACs is even higher than that in SACs because the experimental synthesis and characterization methods for SACs are more mature, and the mechanisms for heterogeneous catalysis on single active sites are so far more comprehensively studied compared with those on dual-metal sites. In this section, we provide a brief introduction to these approaches and their applications in investigating DACs and provide future perspectives.
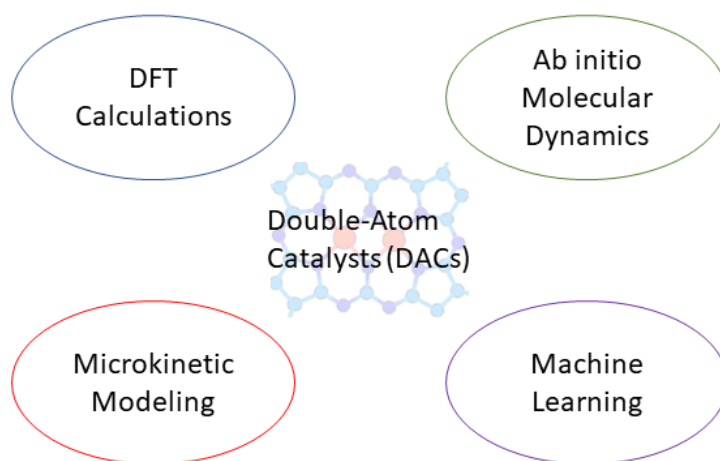

Figure 7. Schematic of widely used computational methods for the rational design of DACs.

First-principles (or *ab initio*) DFT calculations based on the theory developed by Kohn *et al.*[36] have found wide applications in studying the mechanism of heterogeneous catalysis owing to the accurate description of atomic structures and electronic, magnetic, and optical properties, which are comparable to those obtained experimentally.[37] One of the most important applications in catalysis is the calculation of the Gibbs free energy change and overpotential values from DFT-calculated total energy values, which can be used to determine the catalytic performance and

possible reaction pathways in heterogeneous catalysis.[35] Generally, the Gibbs free energy change, ΔG, for each intermediate in the catalytic reactions can be defined as[38]

$$\Delta G = \Delta E + \Delta ZPE - T\Delta S + \Delta G_U + \Delta G_{pH},$$

where ΔE, ΔZPE, and $T\Delta S$ represent the changes in the DFT-calculated electronic energy, zero-point energy, and entropic contribution, respectively; ΔG_U is the Gibbs free energy contribution of electrode potential U; and ΔG_{pH} is the correction due to the pH values. Typically, the Gibbs free energy diagram is constructed from calculated ΔG values and the reaction step with the highest ΔG is determined as the potential-limiting step (PLS), which is used to calculate the theoretical overpotential value for a reaction.[38b, 38c, 39] An important factor in the design of catalysts is the determination of descriptors. The Sabatier principle in heterogeneous catalysis indicates that an ideal catalyst should bind molecules and intermediates that are neither too strong nor too weak;[40] in addition, the so-called scaling relations imply that the adsorption energies of intermediates in multistep reactions such as ORR, NRR, and CO_2RR may correlate with each other.[37b, 41] Consequently, a small set of descriptors based on the adsorption free energy ΔG for key intermediates, instead of adsorption free energies of all reactants, is widely used. In addition to the Gibbs free energies, the underlying origin of the different adsorption strengths and catalytic performances of the catalysts need attention. Moreover, the electronic properties stemming from the DFT-calculated total and partial density of states, band structures, and crystal orbital Hamiltonian population (COHP)[42] are widely applied to describe the intrinsic properties of catalysts. The well-established d-band theory is an example of an outstanding descriptor that links the electronic structure to adsorption strength, and finally to catalytic activity.[43] Other descriptors such as the peak position of the valence band[44], the position of the lowest unoccupied state[45], and integrated COHP[46] are also extracted from electronic structure calculations to provide a

proper description of catalytic activities.[47] As for DACs, distinctive descriptors based on the interaction between the metal atoms in a dimer, local coordination environment (e.g., van der Waals radii of atoms and bond length), and intrinsic properties of metal atoms (e.g., the number of valence electrons, electronegativity, and electron affinity), like those for SACs,[48] are still lacking. This may become an appealing research topic in the future.

Stability is an important issue in the construction of DACs. In theoretical calculations, to examine whether metal aggregation can be suppressed to form stable atomically dispersed structures in DACs, the adsorption energy of metal dimers onto the substrate (or formation energy) is compared with the cohesive energy of metal atoms in their bulk form. Guo *et al.* proposed two descriptors for the thermodynamic and electrochemical stability of DACs: formation energy $E_f = (E_{MM'-sub} - E_{sub} - E_M - E_{M'})$ and dissolution potential $U_{diss} = U_{diss}^0(\text{metal, bulk}) - E_f/ne$, where E_M denotes the total energy of metal atom M in the most stable bulk, E_{sub} denotes the total energy of the substrate, $U_{diss}^0(\text{metal,bulk})$ represents the standard dissolution potential of bulk metal, and n is the number of transferred electrons in the dissolution process.[18, 49] Negative E_f and positive U_{diss} indicate stability, and the agreement between the authors' predictions and experimental results confirm the validation of the method.[18, 49] In addition, AIMD simulations are commonly conducted to check whether the double-atom structure can be maintained at a certain temperature and chemical environment.[50]

The microkinetic modeling method complements DFT calculations in the determination of rate constants and concentration effects in heterogeneous catalysis, which can be experimentally measured and verified, including turnover frequency (TOF) and selectivity toward the desired products.[51] In the microkinetic simulations, a reaction network containing all the intermediate steps in the reaction is constructed, followed by a set of equations to be solved numerically with

initial concentration to obtain the time-dependent concentration evolution of each species. Owing to the relatively low computational cost, microkinetic modeling can open up new pathways for analyzing experimental results and provide predicting power; thus, it can act as a powerful tool for probing the catalytic activity of DACs.[52]

ML, a recently emerged multidisciplinary approach, can greatly expedite materials design and thus the discovery of new materials. Notably, ML approaches have been applied in the energy-related field,[53] with applications including, but not limited to, batteries,[54] solar cells,[55] and catalysts.[56] For catalysis, conventional quantum chemistry methods can provide a large data set of information for catalytic systems, but the formidable computational cost severely hinders further screening processes. ML methods, on the other hand, can furnish the catalyst design process with a fast and efficient tool for evaluating the key features linking the structural information and catalytic performance. The basic procedure for ML includes data collection, feature engineering, and selection of the ML algorithm.[53b] In a pioneering work, Zhu and coworkers applied the gradient boosted regression (GBR) ML algorithm to investigate the possible fundamental factors governing the catalytic performance of TM_1/TM_2-N_6-C DACs for ORR.[52a] The data set comprised fundamental parameters for TM atoms, such as the total number of electronegativities, first ionization energies, and the number of d electrons. After evaluating these key features using the GRB algorithm, precise predictions of ΔG_{OH*} (a descriptor for ORR) from ML, which is in good agreement with the DFT-calculated results, were achieved. However, other ML algorithms, such as ridge regression, K-nearest neighbor regression, support vector regression, random forest regression, and feed-forward neural network regression, show large discrepancies between predicted and DFT-calculated ΔG_{OH*}, indicating that these methods are not as accurate as is GBR. This work paved a new way for using ML algorithms to predict the catalytic activity of DACs
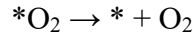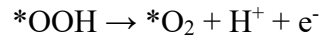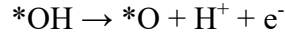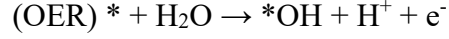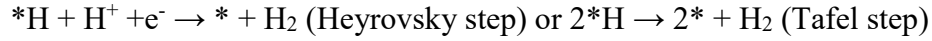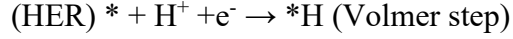
without prior large-scale DFT calculations. Nevertheless, more research combining ML and DFT is still in great demand for other catalytic reactions, such as OER, NRR, and CO_2RR. Considering the much larger data set with many combinations provided by the dual-site nature for DACs as compared with SACs, combining ML and DFT to analyze the intrinsic behavior of DACs is expected to be an intriguing research topic.

4. Practical Applications of DACs in Heterogeneous Catalysis

In this section, we will focus on the progress and challenges of DACs in heterogeneous catalysis with applications in water splitting, ORR, NRR, CO_2RR, and other catalytic reactions. For each reaction, we will first introduce the reaction mechanism and obstacles in improving the catalytic performance, followed by introducing the recent advances in DACs, with both experimental and theoretical investigations.

4.1 Water Splitting

Hydrogen is highly attractive for substituting fossil fuels because of its high mass energy density and pollution-free energy carrier nature, and effective hydrogen production is among the key elements for utilizing hydrogen energy.[6b, 6d, 35, 57] Water electrolysis driven by electrochemical or photochemical water splitting (with the general formula of $H_2O \rightarrow H_2 + 1/2O_2$) is a sustainable way to convert electrical or solar energy into energy stored in hydrogen molecules by hydrogen production. In principle, water splitting involves two half-cell reactions: HER on the cathode of the electrolyzer and OER on the anode.[35] The prevailing mechanisms for the HER and OER in an acidic medium are:[58]

$$(\text{HER}) * + H^+ + e^- \rightarrow *H \text{ (Volmer step)}$$

$$*H + H^+ + e^- \rightarrow * + H_2 \text{ (Heyrovsky step) or } 2*H \rightarrow 2* + H_2 \text{ (Tafel step)}$$

$$(\text{OER}) * + H_2O \rightarrow *OH + H^+ + e^-$$

$$*OH \rightarrow *O + H^+ + e^-$$

$$*O + H_2O \rightarrow *OOH + H^+ + e^-$$

$$*OOH \rightarrow *O_2 + H^+ + e^-$$

$$*O_2 \rightarrow * + O_2$$

And those in an alkaline medium are:

$$(\text{HER}) * + H_2O + e^- \rightarrow *H + OH^- \text{ (Volmer step)}$$

$$*H + H_2O + e^- \rightarrow * + OH^- + H_2 \text{ (Heyrovsky step) or } 2*H \rightarrow 2* + H_2 \text{ (Tafel step)}$$

$$(\text{OER}) * + OH^- \rightarrow *OH + e^-$$

$$*OH + OH^- \rightarrow *O + H_2O + e^-$$

$$*O + OH^- \rightarrow *OOH + e^-$$

$$*OOH + OH^- \rightarrow *O_2 + H_2O + e^-$$

$$*O_2 \rightarrow * + O_2$$
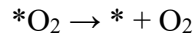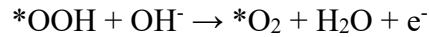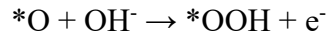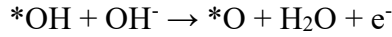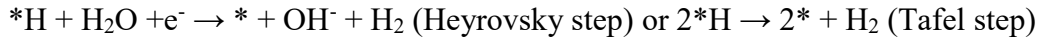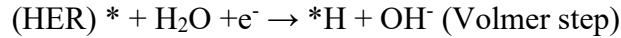
For water splitting, the standard potential is 0 V for hydrogen electrode and 1.23 V for oxygen electrocatalysis versus reversible hydrogen electrode (RHE) at 1 bar pressure and 298 K.[59] Kinetically, the rates of HER and OER are low because of their high energy barriers; thus, the development of novel electrocatalysts or photocatalysts is required for water splitting.[6e, 60] DACs,

because of their synergistic effect that can enhance the catalytic activity, as well as the high AUE and selectivity originating from the atomically dispersed nature, can serve as potential candidates for HER,[25b, 26b, 61] OER,[19, 32, 62] and overall water splitting (**Table 1**).[63]

First, we focus on the practical applications of DACs in HER. In 2019, Zhang *et al.* reported the use of an ALD method to prepare Pt/Ru dimers supported on NCNTs (**Figure 2b**).[25b] Atomic resolution HAADF-STEM clearly illustrated the metal dimer structure with different contrast (**Figure 8a**), confirming the heteronuclear nature of the as-prepared Pt-Ru DACs. In 0.5 M H_2SO_4 at room temperature, the linear sweep voltammetry measurement results of Pt-Ru DACs were compared with those of Pt SACs and commercial Pt/C catalysts. Pt-Ru DACs exhibited the best HER performance among the three catalysts (**Figure 8b**). Furthermore, the HER activity per unit mass at 0.05 V overpotential was 23.1 A mg^{-1} for Pt-Ru DACs, 54 times greater than that for Pt/C (0.43 A mg^{-1}) (**Figure 8c**). Compared with that adsorbed by nanoparticle catalysts, DACs may adsorb more than one hydrogen atom per site in the dimers. DFT calculations showed that the Pt-Ru dimers can adsorb up to six hydrogen atoms (**Figure 8d**), while AIMD simulations revealed the thermal stability of such a structure. To evaluate the theoretical HER performance, the hydrogen adsorption Gibbs free energy change (ΔG_H) was used as a universal descriptor, where a ΔG_H value close to 0 indicates that hydrogen can bind to the catalyst surface neither too strong nor too weak, thus exhibiting the optimum HER activity.[35] According to these results, ultralow ΔG_H of 0.01 eV was identified for the reaction step of Pt(3H)Ru(3H)→→Pt(3H)Ru(2H) (**Figure 8e**), compared with 0.14 eV for Pt-Pt DACs, suggesting the significant role of Ru in the DACs. Further electronic structure analysis showed that the synergistic effect induced by Pt can further modulate the H-Ru bonding, leading to outstanding HER activity. Chao *et al.* synthesized Pt-Cu DACs on palladium nanorings with a two-step approach, and this catalyst showed remarkable HER activity

(small overpotential of 22.8 mV at a current density of 10 mA cm^{-2}) with only 1.5 atom% Pt content.[61a] By "single-atom to single-atom" grafting, Zeng *et al.* fabricated the active moiety Pt$_1$@Fe-N-C from Pt atoms and Fe-N$_4$ moieties.[63] The DACs exhibited remarkable overall water splitting activity, with HER overpotential of 60 mV and Tafel slope of 42 mV dec^{-1}, in acidic media at a current density of 10 mA cm^{-2}, and these values are comparable to those obtained using commercial Pt/C.

Table 1. Summary of DACs with the corresponding catalytic activity for water splitting.

Catalyst	Reaction	Metal content (wt%)	Electrolyte	Overpotential at 10 mA cm^{-2} (mV)	Tafel slope (mV dec^{-1})	Publication year
Cu-Pt nanorings	HER	-	0.5 M H$_2$SO$_4$	22.8	25	2017[61a]
Pt$_1$@Fe-N-C	HER	Pt 2.1; Fe 1.1/1.0 (XPS/ICP)	0.5 M H$_2$SO$_4$/1 M KOH	60 (acidic)	42 (acidic)	2018[63]
Pt-Ru/NCNTs	HER	Pt 0.9; Ru 0.31 (ICP-OES)	0.5 M H$_2$SO$_4$	-	38.9	2019[25b]
A-CoPt-NC	HER	-	0.5 M H$_2$SO$_4$/1 M KOH	27 (acidic)/50 (alkaline)	31 (acidic)/48 (alkaline)	2019[26b]
W$_1$Mo$_1$-NG	HER	W 5.01; Mo 2.55 (ICP-MS)	0.5 M H$_2$SO$_4$/1 M KOH	24 (acidic)/67 (alkaline)	30 (acidic)/45 (alkaline)	2020[61b]
FeTPyP (pyridyl-porphyrin)-Co	OER	-	0.1 M NaOH	310	-	2016[64]

Pt$_1$@Fe-N-C	OER	Pt 2.1; Fe 1.1/1.0 (XPS/ICP)	0.1 M KOH	310	62	2018[63]
Ir-DHC on α-Fe$_2$O$_3$	OER	-	0.1 M KNO$_3$ (pH = 6)	-	-	2018[32]
Co-Fe-N-C	OER	Co 9.4×10^{-8}; Fe 8.6×10^{-9} mol/cm^2 (ICP-AES)	1 M KOH with 10 ppm Fe(NO$_3$)$_3$·9H$_2$O	309	37	2019[19]
CoNi-SAs/NC	OER	-	0.1 M KOH	340	58.7	2019[62b]
CoDNi-N/C	OER	Co 0.30; Ni 0.21 (XPS)	0.1 M KOH	310	72	2019[62a]
Fe-NiNC	OER	Fe 0.33; Ni 0.57 (ICP-MS)	1 M KOH	340	54	2020[62c]
Fe$_2$-GNCL	OER	Fe 0.47 (XPS)	1 M KOH	355	66	2020[65]
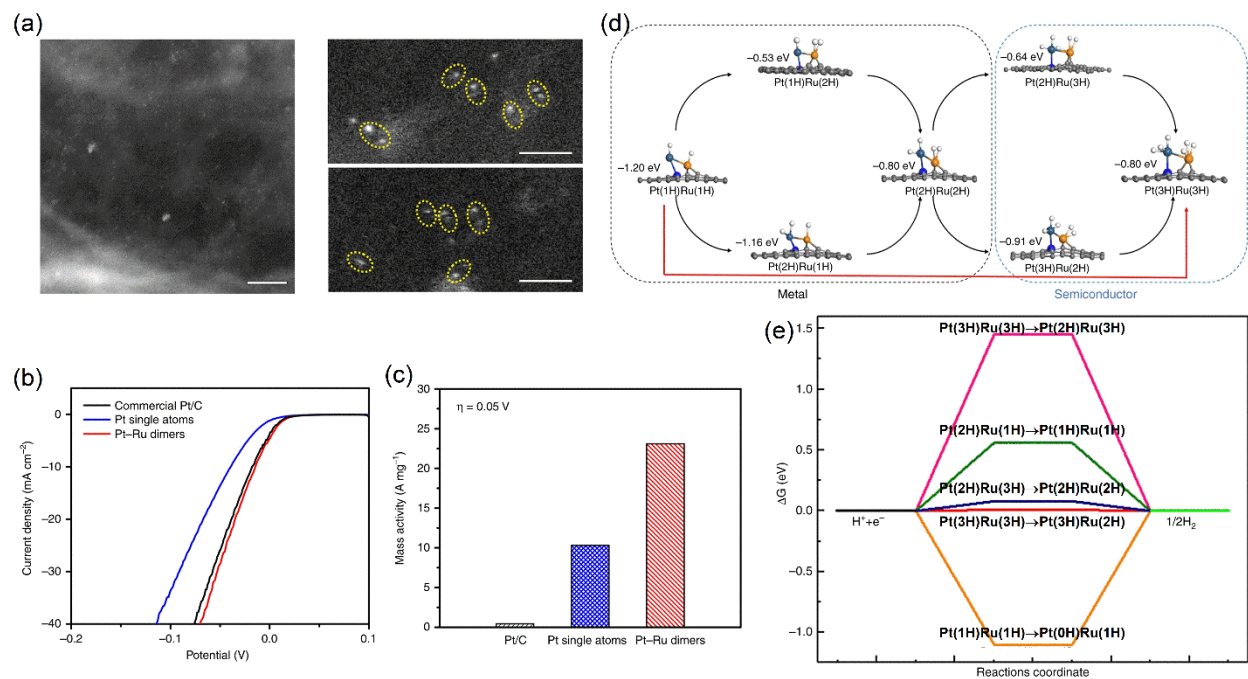
Figure 8. Catalytic activity and characterization of DACs for HER. (a) Aberration-corrected HAADF-STEM images for Pt-Ru/NCNTs, (b) HER polarization curves, and (c) normalized mass activity at 0.05 V for Pu-Ru DACs, Pu SACs, and Pt/C catalysts, (d) atomic structure of different H adsorption configurations on the Pt-Ru dimer, and (e) schematic of ΔG_H for different H coverage of typical configurations. Here, Pt(nH)Ru(mH) represents *n* hydrogen atoms adsorbed on Pt and *m* hydrogen atoms adsorbed on Ru site. Reproduced and adapted with permission.[25b] Copyright 2019, Nature Publishing Group.

Non-Pt-based DACs can also act as promising HER electrocatalysts. In 2020, O-coordinated heteronuclear W-Mo DACs anchored on N-doped graphene (NG; W_1Mo_1-NG) were synthesized by a self-assembly and nitridation method with precise control.[61b] This DAC exhibited high HER activity in both acidic (overpotential of 24 mV at a current density of 10 mA

cm^{-2}; Tafel slope of 30 mV dec^{-1}) and alkaline environments (overpotential of 45 mV at a current density of 10 mA cm^{-2}; Tafel slope of 67 mV dec^{-1}) and outstanding stability, which can be ascribed to the near-optimum ΔG_H value induced by the synergistic effect of DACs, as verified by the DFT calculations.

The overall efficiency of water splitting is limited by the sluggish four protons and electrons transfer kinetics in the OER, which is generally considered as the bottleneck for water splitting.[6b, 7] Considerable efforts have been put into searching for highly efficient OER catalysts, among which SACs are potential candidates.[14b, 66] However, their OER performance is still limited by the scaling relations due to the multistep nature of OER, and more in-depth fundamental research is in great demand. The OER in an alkaline medium is a reaction that can benefit from bimetallic promotion. To be more specific, partial substitution of TM atoms to form bimetallic catalysts (especially those containing Fe[67]) can lead to enhanced OER performance.[7, 38b, 39] In this regard, Bai *et al.* fabricated Fe-Co DACs (Co-Fe-N-C) from a single-atom Co precatalyst (Co-N-C) through an in situ electrochemical method (Fe incorporation by addition of 10 ppm Fe(NO$_3$)$_3$·9H$_2$O to the normal KOH electrolyte).[19] The OER performance was significantly increased upon Fe incorporation, along with a decrease in the overpotential from 443 to 309 mV at a current density of 10 mA cm^{-2} and a decrease in the Tafel slope to 37 mV dec^{-1} (**Figure 9a,b**). To further elucidate the local structure and environment of the as-fabricated DACs, operando XAS was applied to DACs both before and during catalysis. From the EXAFS spectra at the Co K-edge, two coordinated shells, attributed to single scattering paths of the closest C, N, and O (1.5–2 Å) and outer neighboring C and metal surrounding the absorbing cobalt ions (2–3 Å), were identified (**Figure 9c**). After activation, the extracted structural parameters were obtained from the EXAFS results, together with the newly formed Co-Fe scattering path (~2.51 Å), confirming the proposed

structure model with novel Co-Fe interaction (**Figure 9d**). The results indicate that Co-N-C undergoes structural changes when in contact with the alkaline electrolyte and interacts with Fe to form Co-Fe DACs, which show high TOFs (**Figure 9e**). This work indicated that DACs could offer an appealing platform for designing molecularly defined, easily accessed, and earth-abundant bimetallic catalysts for OER. In addition, DACs including Co-Ni[62a, 62b] and Fe-Ni[62c] embedded in NC materials exhibited high bifunctional catalytic activity (OER/ORR). For instance, atomically dispersed Co-Ni DACs were fabricated by controlled pyrolysis of MOFs, and the as-designed CoNi-SAs/NC catalysts delivered remarkable bifunctional activity and long-term durability.[62b] For OER, the overpotential value of 340 mV and Tafel slope of 58.7 mV/dec for Co-Ni DACs were lower than those for CoNi nanoparticles, indicating improved OER activity. DFT studies confirmed that the Co-Ni dual sites, compared with Ni single sites, can result in a reduced OER energy barrier and faster reaction kinetics, explaining the enhanced catalytic activity.
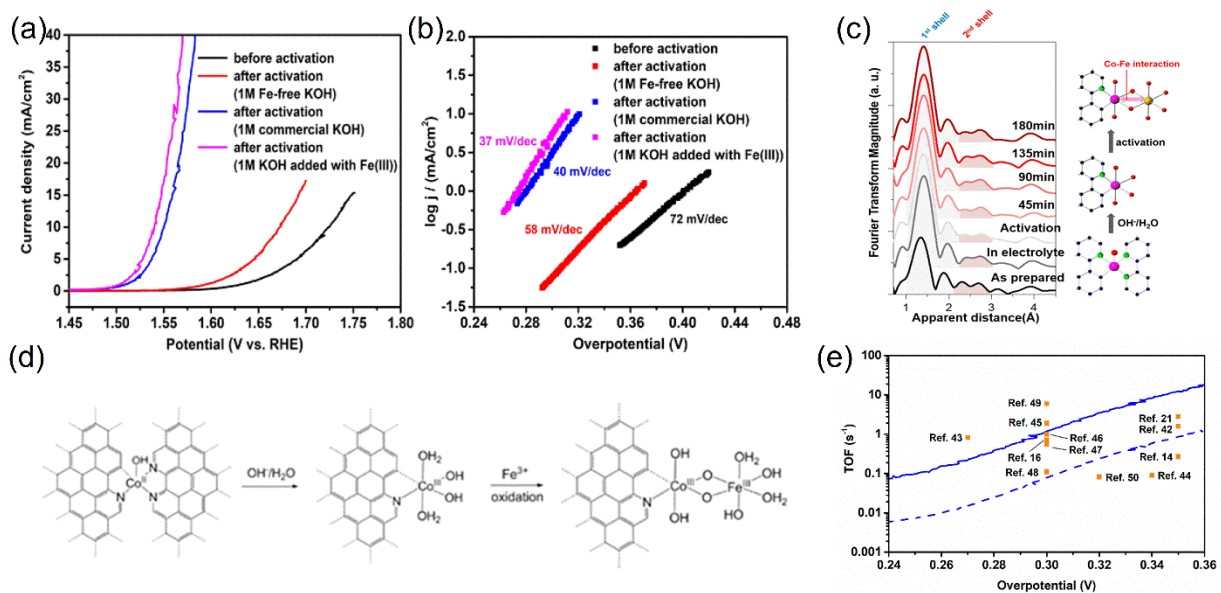
Figure 9. Catalytic activity and characterization of DACs for OER. (a) Linear sweep voltammetry scans and (b) corresponding Tafel slope for Co-N-C before and after KOH treatment. (c) Fourier transform of Co K-edge EXAFS spectra of catalysts before and under OER for various durations, (d) proposed model for the formation of Co-Fe DACs, and (e) potential-dependent turnover frequencies (TOFs) of Co-Fe-N-C (the solid line and dashed line are based on the loadings of Co-Fe sites and the loadings of total metals, respectively) compared with literature. Reproduced with permission.[19] Copyright 2019, American Chemical Society.

In addition to the electrocatalytic OER, DACs showed high competence for solar water oxidation. Zhao and coworkers reported DACs consisting of two Ir metal cations bonded to the α-Fe_2O_3 support stably through a photochemical method.[32] Aberration-corrected HAADF-STEM clearly demonstrated the double-atom nature of the catalysts (**Figure 5**). The Ir DACs showed remarkable catalytic activity, with the TOF value per atom being 2.6 and 5 times higher than those of Ir SACs and Ir nanoparticles, respectively. Moreover, no noticeable degradation in the chronoamperometry can be observed after 10 h, and key features of data from STEM, in situ diffuse reflectance infrared Fourier transform (DRIFT), and XPS after the test were similar to those obtained before the test, indicating that Ir DACs have remarkable stability.

Theoretical calculations also play an important role in designing DACs for water splitting. Liu and coworkers studied the HER mechanism for DACs on NG by DFT calculations.[68] They used water dissociative chemisorption energy as a descriptor for alkaline HER and identified promising DAC—PtRu@NG for acidic HER with a low ΔG_H of -0.07 eV. Instead of 2D materials or their heterostructures, Mohajeri *et al.* studied the potential water splitting applications of DACs using a finite-size quasi-planar cluster B_{38} as the support.[69] According to their DFT calculations,
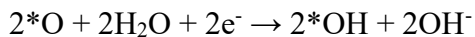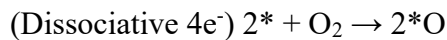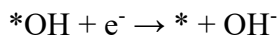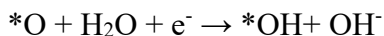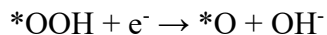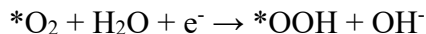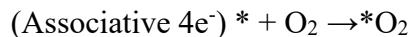
four DACs, namely, FeCr, FeCo, FeNi, and FeCu, on B_{38} exhibited high bifunctional activity for both HER and OER. Specifically, FeNi@B_{38}, due to the strong synergistic effect with the feasibility of OER on Fe sites and HER on Ni sites, is the most promising bifunctional catalyst among the investigated DACs. Li *et al.* designed DACs using two adjacent metal-N_3 / metal-N_4-C_{60} moieties, which can break the intrinsic scaling relations in OER and ORR.[70] For ORR, compared with the universal linear scaling relation $\Delta G_{OOH} = \Delta G_{OH} + 3.2$ eV, the dual-metal-N_3 DACs can bond *OOH* more strongly without affecting *OH bonding, leading to a new relation $\Delta G_{OOH} = \Delta G_{OH} + 2.41$ eV and much improved limiting potential surpassing that for SACs and even Pt(111). For OER, on the other hand, the O_2 molecules can be formed through a new mechanism from two adsorbed O atoms rather than the conventional dehydrogenation of *OOH, leading to optimum theoretical OER activity with an overpotential of 0.08 V on dual CoN_4-C_{60}. This work highlights the potential of DACs in circumventing the scaling relations toward improved catalytic performance beyond the limitation of single-site catalysts, and this method could be extended to other catalytic reactions such as CO_2RR.[50]

4.2 ORR

Proton-exchange membrane fuel cells, also known as polymer electrolyte membrane fuel cells (PEMFCs), are considered one of the most promising next-generation energy solutions in transportation applications and other devices because of their high energy conversion efficiency and environmentally friendly characteristics.[8c, 71] ORR, as the cathode reaction of PEMFC, shows more sluggish kinetics than does the hydrogen oxidation reaction, the anode reaction of PEMFC, and therefore is considered as the kinetic limitation for PEMFC performance and the key obstacle in the large-scale industrialization of PEMFCs.[8c, 28a, 34] In addition, ORR determines the output

energy capacity of rechargeable metal-air batteries.[72] Consequently, ORR is regarded as one of the most important catalytic processes in energy conversion research. Pt, as the benchmark catalyst for ORR, exhibits high activity, but its high cost and natural scarcity hinder its industrial application.[72] Solutions to overcome this obstacle include exploring non-precious alternatives for Pt-based electrodes and downsizing the metal particles to the atomic scale. Atomically dispersed SACs have been widely recognized as alternatives to replace Pt in fuel cells and metal-air batteries, while efforts including engineering the coordination environment of single atoms and the electronic structure and porosity of the substrate have been applied to further improve the ORR activity.[8d, 73] Introducing the synergistic effect of metal dimers by replacing SACs with DACs is another promising strategy, where experiments and simulations work in close collaboration to examine potential ORR catalysts.

It is well known that ORR mechanisms include the $4e^-$ process toward H_2O/OH^- and $2e^-$ process toward H_2O_2/HO_2^-.[8b, 34, 73] As an example, in an alkaline medium, the mechanisms for $4e^-$ and $2e^-$ processes including the intermediates are (* denotes active sites):[34-35, 38a]

$$(\text{Associative } 4e^-) * + O_2 \rightarrow *O_2$$

$$*O_2 + H_2O + e^- \rightarrow *OOH + OH^-$$

$$*OOH + e^- \rightarrow *O + OH^-$$

$$*O + H_2O + e^- \rightarrow *OH + OH^-$$

$$*OH + e^- \rightarrow * + OH^-$$

$$(\text{Dissociative } 4e^-)\ 2* + O_2 \rightarrow 2*O$$

$$2*O + 2H_2O + 2e^- \rightarrow 2*OH + 2OH^-$$

$$2*OH + 2e^- \rightarrow 2* + 2OH^-$$

$$(2e^-) * + O_2 \rightarrow *O_2$$

$$*O_2 + H_2O + e^- \rightarrow *OOH + OH^-$$

$$*OOH + e^- \rightarrow * + OOH^-$$
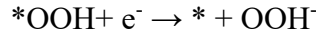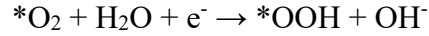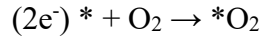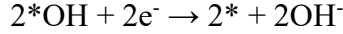
While the $2e^-$ process is used for H_2O_2 production, the $4e^-$ process is preferred in fuel cell applications because it can lead to high current efficiency.[34] The selectivity toward $4e^-$ can be determined by the DFT-calculated adsorption energy of $*OOH$[74] therefore, combining experiments and theory is crucial in the design of ORR catalysts. From a thermodynamic point of view, finding suitable catalysts to break the O-O bond with low energy barriers can lead to enhanced ORR activity. DACs may provide an opportunity because the dual-site structure may result in an energetically preferential side-on adsorption pattern with an elongated O-O bond, reducing the O-O bond cleavage barrier and enhancing the theoretical ORR performance. Inspired by this, introducing another metal site to form atomically dispersed dimers for ORR has become an appealing topic.

In the past five years, several DACs have been reported for ORR, and most of the experimentally realized DACs were supported on carbon materials, especially N-C,[26a, 28a, 28d, 62, 75] (**Table 2**) because of their outstanding electrical conductivity, highly exposed active sites, and ultrahigh porosity.[76] Homonuclear DACs including Co[75b] and Fe pairs[28d] anchored on N-C, which were synthesized through the precise tuning of metal loading, have been demonstrated as highly efficient ORR electrocatalysts. By controlling the atomic-scale structure of the bimetal–organic framework before pyrolysis through a self-adjusted strategy, Xiao *et al.* successfully fabricated $Co_2N_xC_y$ homonuclear DACs. The dual sites were characterized by aberration-corrected

STEM and XANES, while the Co_2N_5 structure was identified through DFT calculations.[75b] The designed structure presented a much higher ORR activity than that of the single-atom CoN_4 site, which was proven by the 12-times-higher mass activity for Co_2N_5 than that for CoN_4. On the other hand, Fe_2 clusters on N-C were selected by Ye and coworkers, who used a two-step synthetic process to produce the catalysts.[28d] They designed a separated cavity in ZIF by encapsulating the $Fe_2(CO)_9$ compound before pyrolysis to prevent metal aggregation. Fe_2-N-C exhibited a remarkable acidic ORR activity with a half-wave potential ($E_{1/2}$) of 0.78 V versus RHE and excellent durability with only a -20 mV shift after 20,000 cycles.

Table 2. Summary of DACs with the corresponding catalytic activity for ORR.

Catalyst	Metal content (wt%)	Electrolyte	Onset potential E_{onset} (V)	Half-wave potential $E_{1/2}$ (V)	Kinetic current density J_K (mA cm^{-2})	Publication year
(Fe,Co)/N-C	Fe 0.93; Co 1.17 (ICP-AES)	0.1 M HClO$_4$	1.06	0.863	2.842 (0.9 V)	2017[28a]
FeCo-NPC	Fe 0.43; Co 0.37 (ICP-AES)	0.1 M HClO$_4$/0.1 M KOH	0.97 (alkaline); 0.85 (acidic)	0.87 (alkaline); 0.74 (acidic)	11.48 (0.85 V, acidic); 7.80 (alkaline)	2017[77]
A-CoPt-NC	Co 1.72; Pt 0.16 (ICP-AES)	0.1 M KOH	-	0.96	-	2018[26a]
(Fe,Co)/CNT	Fe 1.21; Co 1.13 (ICP-AES)	0.1 M KOH	1.15	0.945	17.51 (0.9 V)	2018[78]
Co$_2$N$_5$/C (Co-N-C-10)	Co 1.06 (XPS)/4.3 (ICP)	0.1 M HClO$_4$	0.92	0.79	-	2018[75b]

Pt$_1$@Fe-N-C	Pt 2.1; Fe 1.0 (ICP-OES)	0.5 M H$_2$SO$_4$	0.93	0.80	-	2018[63]
FeCo/CN	Fe 0.964; Co 0.218 (ICP-OES)	0.1 M KOH	0.995	0.920	31.1 (0.88 V)	2018[75a]
Zn/CoN-C	Zn 0.33; Co 0.14 (ICP-MS)	0.1 M KOH/HClO$_4$	1.004 (alkaline) 0.97 (acidic)	0.861 (alkaline) 0.796 (acidic)	-	2019[75c]
CoNi-SAs/NC	-	0.1 M KOH	0.88	0.76	23.2 (0.5 V)	2019[62b]
Fe$_2$-N-C	Fe 0.38 (ICP-MS)	0.5 M H$_2$SO$_4$ /0.1 M KOH	-	0.78 (acidic) 0.905 (alkaline)	16.4 (0.75 V)	2019[28d]
CoPNi-N/C	Co 0.17; Ni 0.02 (XPS)	0.1 M KOH/HClO$_4$	0.93 (alkaline) 0.86 (acidic)	0.84 (alkaline) 0.72 (acidic)	5.4 (0.4 V, alkaline) 6.2 (0.4 V, acidic)	2019[62a]
FeCoN$_5$/C	Fe 1.06; Co 1.12 (XPS)	0.1 M HClO$_4$	1.02	0.86	16.07 (0.8 V)	2019[79]

FeCo@C	Co 0.5; Fe 0.37 (ICP-AES)	0.1 M KOH/0.5 M H_2SO_4	0.98 (alkaline)	0.89 (alkaline)	-	2019[28b]
(Zn,Co)/NSC	Zn 0.13; Co 0.26 (XPS)	0.1 M KOH	1.07	0.893	-	2019[80]
f-FeCoNC	Fe 0.53; Co 0.54 (XPS)	0.1 M KOH	1.05	0.89	-	2019[75d]
Fe-NiNC	Fe 0.33; Ni 0.57 (ICP-MS)	0.1 M KOH	1.0	0.85	-	2020[62c]
Co/Zn-N-C nanofiber	Co 4.89; Zn 4.04 (ICP-MS)	0.1 M $HClO_4$	0.997	0.797	-	2020[75e]
FeCo-IA/NC	Fe 0.26; Co 1.06 (ICP-OES)	0.1 M KOH	0.98	0.88	-	2020[75f]
FeNi-N_6-C	Fe 1.448; Ni 1.472 (ICP-OES)	0.1 M $HClO_4$	-	~0.8	-	2020[81]

Aside from homonuclear DACs, more examples of heteronuclear DACs consisting of distinct adjacent transition metal atom sites exhibit outstanding ORR performance owing to the synergistic effect. Wang *et al.* used the host–guest strategy to design a DAC formed by Fe-Co dual sites supported on N-doped porous carbon, where the bonding between Co nodes (host) and adsorbed Fe ions (guest) is controlled **(Figure 4a)**.[28a] HAADF-STEM, XAFS spectroscopy **(Figure 6)**, and Mössbauer spectroscopy were used to investigate the atomic-scale dual-site structure and coordination environment of (Fe,Co)/N-C DACs. The as-designed DAC exhibited excellent ORR activity with an onset potential (1.06 V) and half-wave potential (0.863 V) that are comparable to those of commercial Pt/C (1.03 V/0.858 V) in the acidic electrolyte. In addition, the kinetic current density of the as-designed DAC was 2.842 mA cm^{-2} at 0.9 V, higher than that of Pt/C **(Figure 10a-c)**. In addition, DFT calculations manifested that the cleavage of the O-O bond happens on Fe-Co dual sites, which can be attributed to strong binding of O_2 (O-O bond length elongated from 1.23 Å to 1.40 Å), therefore leading to high activity (low activation barrier of 0.26 eV) and selectivity toward 4e$^-$ path **(Figure 10d)**. Fe-Co-based DACs were also investigated by Xiao *et al.*, who proposed an OH-ligand self-binding strategy to engineer the adsorption-desorption behavior of catalytic sites.[79] Through DFT calculations and structural characterization by HAADF-STEM and XAS, they confirmed that OH-stabilized $FeCoN_5$ sites were the most promising for ORR, which was later proven by experimental E_{onset} and $E_{1/2}$ values up to 1.02 and 0.86 V, respectively, as well as the 20-time-higher intrinsic activity than that of the single-atom FeN_4 sites **(Figure 10e)**. Besides, H_2O_2 yield was greatly suppressed on FeCo DACs (below 2%) compared with Fe and Co SACs, and the electron transfer number revealed the four-electron ORR pathway on FeCo DACs **(Figure 10f)**. Theoretical calculations further proved that the binuclear center can effectively weaken the binding strength of ORR intermediates and accelerate O-O bond

breaking, leading to enhanced ORR activity (**Figure 10g**). Zhao *et al.* integrated double-atom Fe-Co sites into a 3D carbon network through the fusion-foaming thermal transformation of CoFe@MET-6 nanoparticles (**Figure 4b**), which can serve as a high-performance ORR catalyst with high electrochemical stability.[28b] Zhang *et al*. prepared Fe-Co DACs on MOF-derived N-C by an adsorption-calcination strategy, and the DACs exhibited an $E_{1/2}$ value of 0.92 V, which is 70 mV higher than that of Pt/C.[75a] Chen and coworkers reported the synthesis of Fe-Co dimers on N-doped nanocarbon from MOFs, which exhibited better ORR activity ($E_{1/2}$ value of 0.88 V) and zinc-air battery performance than those obtained using Pt/C.[75f] In addition, Zn-Co,[75c, 75e, 80] Ni-Co,[62a, 62b] and Fe-Ni[62c, 81] atomic pairs have been applied as DACs for ORR and have shown performance comparable to or superior than that shown by Pt/C.
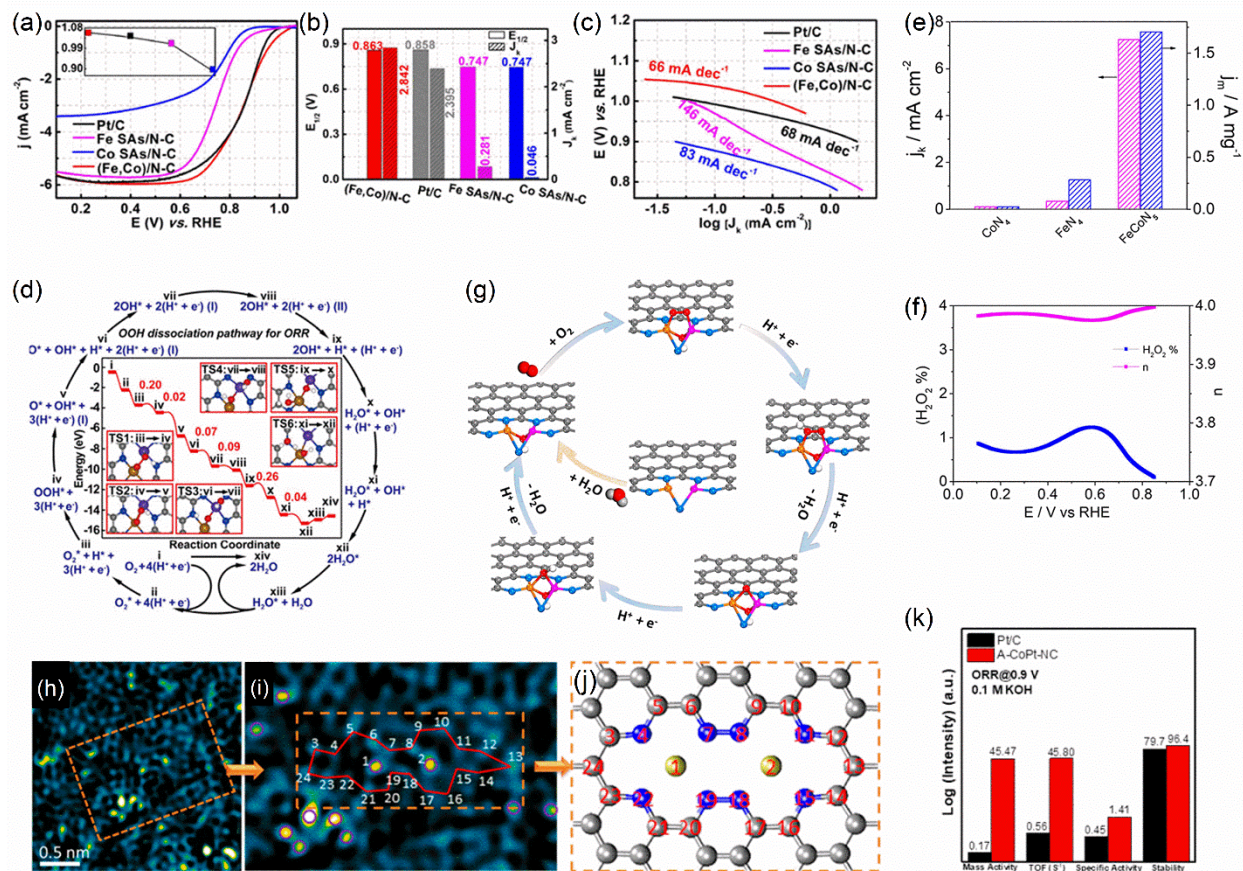
Figure 10. Electrocatalytic performance and characterization of heteronuclear DACs for ORR. (a) Rotating disk electrode polarization curves of Pt/C, Co SAs/N-C, Fe SAs/N-C, and (Fe,Co)/N-C (inset: E_{onset}), (b) comparison of $E_{1/2}$ and J_K, (c) Tafel plots, and (d) energy of intermediates in the mechanism of ORR at (Fe,Co)/N-C from DFT. Reproduced with permission.[28a] Copyright 2017, American Chemical Society. (e) Kinetic current density comparison between $CoFeN_x/C$, CoN_x/C, and FeN_x/C catalysts, (f) H_2O_2 yield and electron transfer number of $FeCoN_x/C$, and (g) the proposed ORR mechanism on $FeCoN_x$-OH site. Reproduced with permission.[79] Copyright 2019, American Chemical Society. (h)(i) HAADF image of A-CoPt-NC after Fourier transformation filtering, (j) the dual-site configuration model, and (k) comparison of ORR activity between A-CoPt-NC and Pt/C. Reproduced with permission.[26a] Copyright 2018, American Chemical Society.

Introducing trace amounts of Pt to form DACs can not only improve the ORR activity compared with that of commercial Pt/C, but also overcome the drawbacks of high cost and scarcity of Pt sources. A-CoPt-NC DACs were fabricated by a two-step method using rod-like Co-MOF precursors (**Figure 3**).[26a] From the HAADF image after Fourier transformation filtering, the local environment and configuration of metal dimers trapped in the defect can be identified (**Figure 10h,j**). Even though the Pt content was only 0.16 wt% (obtained by inductively coupled plasma atomic emission spectroscopy, ICP-AES), A-CoPt-NC exhibited a higher $E_{1/2}$ value (0.92 V), lower limiting current density (4.8 mA cm^{-2}), and mass activity 266 times higher (**Figure 10k**) than those of Pt/C. The 4e$^-$ pathway was found to be predominant in A-CoPt-NC in an alkaline electrolyte, with a H_2O_2 yield below 17%, indicating that the synergistic effect of Co-Pt dimers can result in the energetically favorable breaking of the O-O bond, which is different from that reported for 2e$^-$ pathway for isolated Pt species.[82] From DFT calculations, charge redistribution and shift of the *d* orbital were observed, leading to a highly enhanced ORR performance, which can also be attributed to the synergistic effect.

2D materials with unique physical and chemical properties have emerged as promising heterogeneous catalysts.[34, 83] Metal dimers supported on 2D materials also consist of a large portion of DACs, but currently, experimental evidence is lacking. Recent theoretical investigations fill this gap by predicting that Co-Co on C_2N,[84] Cu-Fe, Ni-Cu,[52a] Co-Pt,[52a] Fe-Co,[85] and Co-Zn[86] on NG and hydroxyl-group-modified metal (Ni, Co, and Fe) dimers on defected graphene[87] are potential candidates for ORR DACs. C_2N monolayers with a size of 0.83 nm and well-ordered vacancies terminated by sp^2-bonded nitrogen atoms can provide enough space to hold metal dimers and are thus promising for constructing stable DACs.[88] In addition, they exhibit good electrical

conductivity. Based on these features, Li and coworkers designed a group of DACs supported on C_2N and examined their ORR activity.[84] Non-noble-metal dimers Co_2, Cu_2, and Ni_2 on C_2N exhibited higher adsorption energy and lower dissociation barrier than those of their single-atom counterparts, which can be further explained by the accumulation of polarization charges (**Figure 11a,b**). Specifically, $Co_2@C_2N$ showed low rate-determining barriers of 0.39 eV along two full ORR pathways, much superior to that of Pt catalysts. Hunter *et al.* screened TM dimers (TM = Co, Pt, Fe, Ni) in NG and constructed an ORR volcano plot of onset potential as a function of ΔG_{*OH} for dimers in two different vacancies: N6V4 and N8V4 (**Figure 11c**); three potential candidates with low overpotential were identified: CoPt, CoNi, and Co_2 on N8V4.[89] The results are consistent with previous experimental observations, where CoPt,[26a] CoNi,[62a, 62b] and Co_2[75b] dimers indeed showed outstanding ORR performance, indicating the validity of DFT calculations in predicting ORR DACs. In addition, COHP analysis showed that for CoPt and CoNi, a much closer-to-optimum antibonding contribution to the interaction between Co and OH forms, leading to optimized ORR energetics.
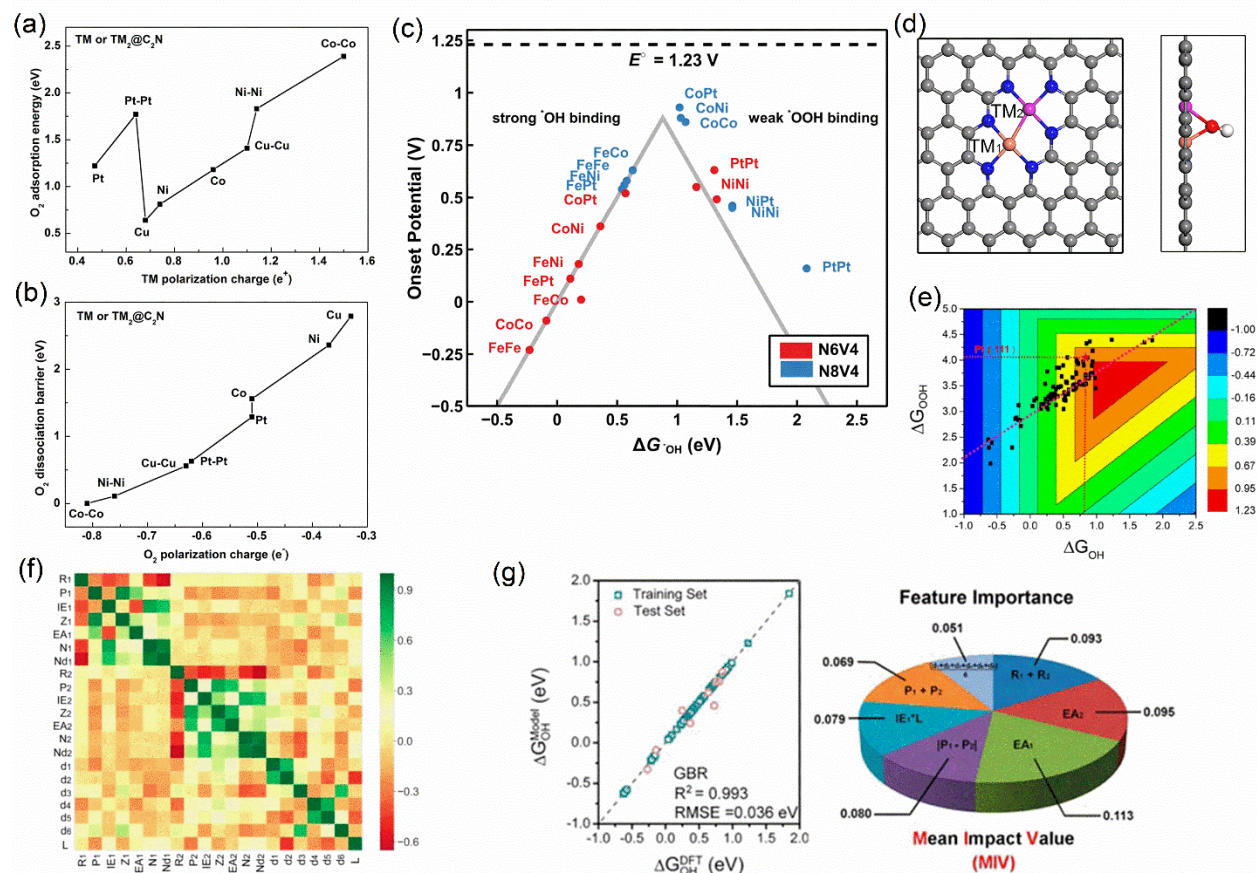
Figure 11. Design of DACs for NRR from theoretical calculations. (a) Dependence of O_2 adsorption energy on TM polarization charge, and (b) dependence of O_2 dissociation barrier on O_2 polarization charge. Reproduced with permission.[84] Copyright 2016, American Chemical Society. (c) ORR volcano plot of onset potential as a function of ΔG_{*OH} for dimers on N6V4 and N8V4 vacancies. Reproduced with permission.[89] Copyright 2016, American Chemical Society. (d) Geometric structure of bare (left) and OH-modified (right) TM_2-N_6-C DACs. (e) Contour plot of ORR activity as a function of ΔG_{OH*} and ΔG_{OOH*}. (f) Heat map of the Pearson correlation coefficient matrix among the selected features for DACs. (g) Comparison of DFT-calculated and ML-predicted ΔG_{OH*} values (left) and feature importance (right). Copyright 2019,[52a] American Chemical Society.

In another intriguing work, Zhu *et al.* combined comprehensive DFT calculations, microkinetic modeling, and ML to scrutinize possible ORR descriptors for TM_2-N_6-C DACs (**Figure 11d**).[52a] Using DFT calculations, they found a linear scaling relationship between ΔG_{OH*} and ΔG_{OOH*} (**Figure 11e**) and also found that ΔG_{OH*} can act as an independent descriptor to describe the ORR activity of DACs. Nevertheless, it would be more intuitive if the ORR activity for DACs can be predicted even prior to the intensive DFT calculations because of its high computational cost. To achieve this, ML algorithms were applied to a large data set consisting of parameters including the total number of valence electrons (N), atomic number (Z), electronegativity (P), first ionization energy (IE), electron affinity (EA), and the number of *d* electrons (N_d) for those DACs (**Figure 11f**). After evaluating the feature importance by the GBR algorithm, seven features with the highest relation to ORR performance were identified, which can predict ΔG_{OH*} values close to the DFT-calculated results (**Figure 11g**). This work provides universal descriptors for ORR on DACs, and the methodology of combining DFT with ML can inspire more theoretical research into investigating descriptors in DACs not only for ORR but also for other catalytic reactions.

Although TM dimers supported on a 3D carbon network and defective 2D NG have been consistently investigated by combining experiments and simulations, to date, the study of other materials as DAC substrates for ORR applications is still in the infancy of research. Further studies may provide more physical and chemical insights into the performance improvement of ORR.

4.3 NRR

NH_3 is an important chemical in both industry and agriculture as it serves as a precursor to various foods, fertilizers, pharmaceuticals, and detergents.[90] Besides, NH_3 is a clean, carbon-free energy carrier whose combustion only produces water and N_2, both of which are environmentally friendly.[91] Therefore, converting N_2—the most abundant gas in Earth's atmosphere, >78%—into NH_3, that is nitrogen fixation, is of vital significance in the Earth's nitrogen cycle.[90b] According to Mineral Commodity Summaries from the US Geological Survey, approximately 170 million tons of NH_3 were produced globally in 2018.[92] A major challenge in nitrogen fixation is breaking the inert N≡N triple bond (bond energy as high as 941 kJ mol^{-1}[93]). The conventional approach of converting N_2 to NH_3 is the Haber–Bosch (H-B) process, which requires high temperature (300–500 °C) and pressure (150–300 atm) and thus is energy-consuming.[9b] Electrocatalytic NRR with the general formula of $N_2 + 6H^+ + 6e^- \rightarrow 2NH_3$, which was first inspired by the biological nitrogen fixation by nitrogenases,[94] is an alternative to the H-B process because NRR can progress under ambient conditions; thus, the requirement for harsh reaction conditions and environmental concerns for the H-B process can be avoided.[9c, 41c, 95]

As an emerging research topic in electrocatalysis, exploring novel catalysts for NRR often requires pioneering guidance from a theoretical perspective. NRR is usually considered a six-net coupled proton and electron transfer (CPET) process (**Figure 12**), where the more energetically favorable pathway between dissociative and associative pathways takes place. In the dissociative pathway, the N≡N bond breaks before the CPET process (**Figure 12a**), whereas in the associative pathway, the N≡N bond breaks only when the first NH_3 molecule is released from the system.[9b] The associative pathway can be further categorized into distal, alternating, and enzymatic pathways based on the N_2 adsorption configuration. For the end-on configuration, the distal or

alternating pathway is adopted (depending on which pathway contains more energetically favorable NRR intermediates, **Figure 12b**), while for the side-on N_2 adsorption configuration, NRR goes through the enzymatic pathway **(Figure 12c)**.[9b, 96] In DFT calculations, the Gibbs free energy values of NRR intermediates were calculated and compared in order to determine the possible NRR pathway as well as the theoretical overpotential.[38c, 96-97].
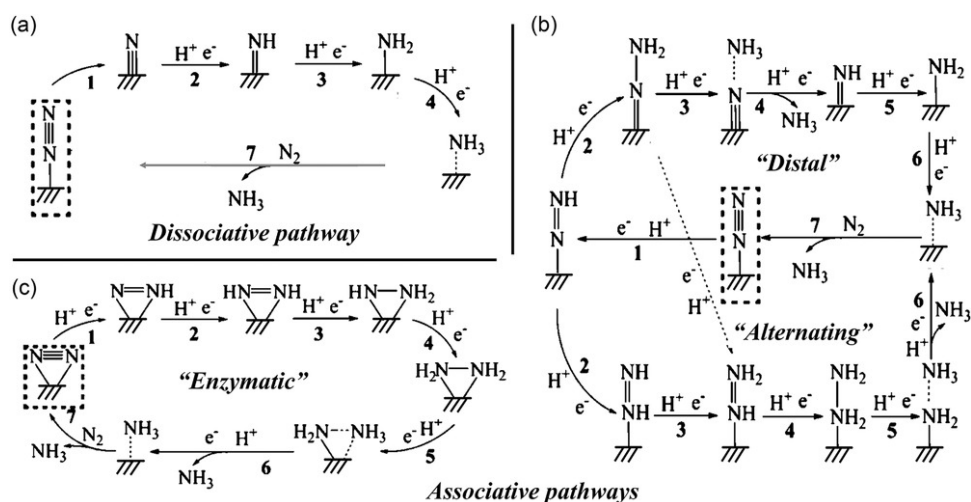
Figure 12. Possible (a) dissociative and (b)(c) associative NRR pathways. Reproduced with permission.[9b] Copyright 2018, Wiley-VCH Verlag GmbH & Co. KGaA, Weinheim.

In addition to the efficient activation of the N≡N triple bond, there are other requirements for an ideal NRR catalyst, such as lowering the reaction energy barrier and suppressing the side reaction HER.[35] Owing to the linear scaling relations that the adsorption energies of nitrogen-related NRR intermediates may have,[41c] some descriptors such as N_2 adsorption energy and Gibbs free energy change for $*N_2 \rightarrow *N_2H$ may exist,[98] which can be used for screening potential NRR catalysts. SACs have been consistently investigated for NRR, both experimentally[16] and

theoretically[38c, 46, 98-99] owing to their large AUE, high stability, and good selectivity. Moreover, for TM-based SACs, the *d* electrons from TM atoms are more active than those in TM bulk or nanoparticles, so that the activation of the N≡N triple bond can be more effective. However, the single-site nature of SACs induces a fundamental bottleneck for enhancing the NRR performance—the scaling relations between the nitrogen-related NRR intermediates, which lead to at least 0.5 V overpotential even near the peak of the NRR volcano plot.[35, 41c] Introducing dimers to tune the adsorption behavior of intermediates in NRR is a possible way to break the scaling relations and form outstanding catalysts that exhibit both high yield rate and high Faradaic efficiency.[18]

It is possibly due to the complexity in the synthesis of suitable DACs for the NRR that the experimental results are only sporadic.[100] By a combination of DFT calculations and experiments, Cao *et al.* designed the doping of strain-induced bi-Ti^{3+} pairs and demonstrated their outstanding NRR performances.[100a] A theoretical study revealed that the adjacent bi-Ti^{3+} sites on anatase (101) serve as the most efficient electrocatalytic centers for NRR compared with single Ti^{3+} sites (**Figure 13a,b**). By doping anatase TiO_2 with Zr^{4+}, the strain effect could induce adjacent bi-Ti^{3+} sites. The as-prepared electrocatalysts showed excellent NRR activity with an NH_3 production rate of 8.90 $\mu g\ h^{-1}cm^{-2}$ and a Faradaic efficiency of 17.3% at -0.45 V *vs.* RHE (**Figure 13c,d**). Li *et al.* synthesized atomically dispersed Fe-Mo dimers in situ anchored on defect-rich graphene (FeMo@NG) by applying the sacrificial template method (**Figure 13e**).[100b] Owing to the synergistic, ligand, and geometric effects, FeMo@NG showed superior NRR activity (yield rate of 14.95 $\mu g\ h^{-1}mg^{-1}$ at -0.4 V and Faradaic efficiency of 41.7% at -0.2 V, **Figure 13f,g**) than that of its single-atom counterparts (Fe@NG and Mo@NG). DFT calculations revealed that $FeMoN_6$ species serve as active sites with relatively lower NRR energy barrier values (0.91 eV) than those

of Fe@NG and Mo@NG through the alternating pathway, contributing to the superior NRR performance.
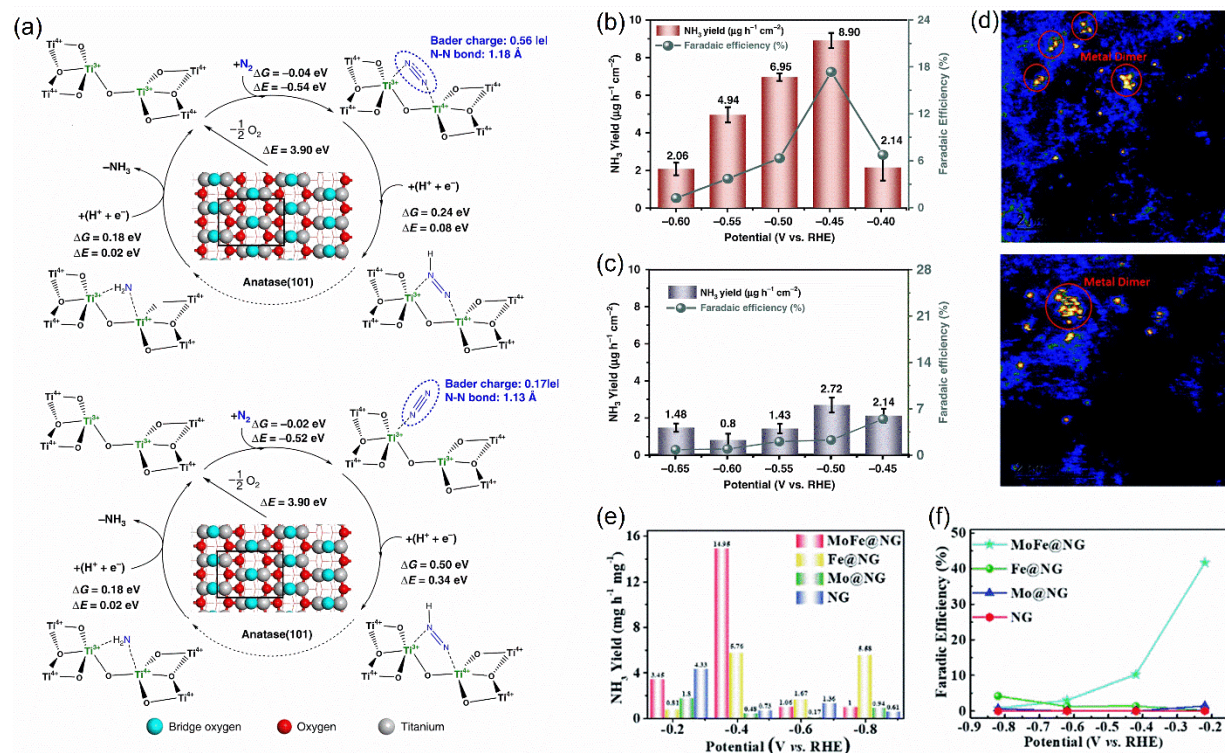
Figure 13. Electrocatalytic activity and characterization of DACs for NRR. DFT-predicted activity for (a) adjacent bi-Ti^{3+} (upper) and single Ti^{3+} (lower) on anatase (101) surface with oxygen vacancy (ΔG and ΔE represent free energy and electronic energy) and experimental NH_3 yield and Faradaic efficiency of (b) Zr-TiO_2 and (c) undoped TiO_2. Reproduced with permission.[100a] Copyright 2019, Nature Publishing Group. (d) HAADF-STEM image of FeMo@NG, (e) NH_3 yield rates and (f) Faradaic efficiencies of FeMo@NG, Fe@NG, and Mo@NG at different potentials. Reproduced with permission.[100b] Copyright 2019, The Royal Society of Chemistry.

Although experimental evidence is scarce, theoretical calculations predict a large group of DACs showing high NRR activity, high selectivity toward NRR over HER, and outstanding stability. DFT-predicted DACs are summarized in **Table 3** with limiting potential (U_L)/overpotential (η) values, reaction pathways, and PLSs listed for each system. Among these reports, Guo *et al.* used *N_2H adsorption energy as a simple descriptor for NRR activity to screen homonuclear and heteronuclear DACs supported on 2D phthalocyanine (M_2-Pc and MM'-Pc, **Figure 14a**) by large-scale DFT calculations.[18] The authors first screened out 25 homonuclear M_2-Pc monolayers with high thermodynamic and electrochemical stabilities, after which N_2 adsorption calculations showed that eight M_2-Pc DACs (M = Cr, Mn, Mo, W, Re, Ti, V, and Ta) can realize strong N_2 chemisorption, which is a prerequisite for NRR catalysts. Furthermore, Gibbs free energy calculations indicated that Ti_2, V_2, and Re_2-Pc can co-balance the adsorption of multiple intermediates in NRR and therefore exhibit outstanding U_L values of -0.75, -0.39, and -0.82 V, respectively (**Figure 14b**), superior to that of the benchmark Ru(0001) (U_L = -0.98 V), which has the highest theoretical NRR activity among the investigated bulk metal surfaces[82b, 97]. They used ΔE_{N2H*} (adsorption energy of N_2H*) as a descriptor for the NRR performance of DACs and found a volcano-shaped relationship between U_L and ΔE_{N2H*} (**Figure 14c**), where V_2-Pc was located near the peak with the highest NRR activity among all the examined DACs. This relationship can be extended to heteronuclear DACs MM'-Pc (M = Ti, V, Ta), where 21 heteronuclear DACs with performance better than that of their homonuclear counterparts were selected (**Figure 14d**). Finally, their selectivity toward NRR rather than the side reaction HER was examined by comparing $\Delta G(H*)$ and $\Delta G(N_2H*)$ (**Figure 14e**), and Ti_2-Pc, V_2-Pc, TiV-Pc, VCr-Pc, and VTa-Pc were found to suppress the competing HER effectively. This work paves the way for screening DACs for NRR with theoretical calculations. In another work, a low NRR

overpotential of 0.21 V with an enzymatic mechanism was predicted for Fe_2/MoS_2 DAC, and the origin of the enhanced performance can be further unraveled by the natural charge population and COHP analysis.[101] The synergistic effect between Fe atoms and the MoS_2 substrate provides electron depletion and vacant orbitals for lone-pair electrons in N_2, and electron back-donation from Fe_2 to N_2 enhances N_2 activation. Other 2D materials, such as graphdiyne,[102] phosphorene,[103] C_2N,[88a, 104] and C_3N_4,[102b] can also serve as substrates for NRR DACs.

Table 3. Summary of DFT-predicted DACs for NRR.

Systems	Best sample	Theoretical limiting potential U_L (V)	Pathway	PLS	Publication year
$TM_2@C_2N$ (TM = Ti, Mn-Co, Cu, Mo, Ru-Ag, Ir-Au)	$Mo_2@C_2N$	-0.41	Distal	*NH→*NH$_2$	2018[104a]
$TM_2@C_2N$ (TM = Cr-Ni)	$Mn_2@C_2N$	-0.23	Enzymatic	*NH-*NH$_2$→*NH$_2$-*NH$_2$	2019[88a]
$TM_2@$graphdiyne (TM = Mn-Ni)	$Co_2@$graphdiyne	-0.43	Distal	*NH$_2$→*NH$_3$	2019[102a]
$TM_2@$phosphorene (TM = Sc-Cu)	$Ti_2@$phosphorene	-0.20	Distal	*NH$_2$→*NH$_3$	2019[103]
Fe-TM@graphene-based substrate (GS)	Fe-Ti@GS	-0.88	Enzymatic	*N$_2$→*N$_2$H	2020[105]

Fe$_2$@C-DV/G, N-DV/G, g-C$_3$N$_4$, GDY	Fe$_2$@g-C$_3$N$_4$	-0.32	Enzymatic	*N$_2$→*N$_2$H	2020[102b]
TM$_1$TM$_2$@N-doped porous graphene	FeRh@N-doped porous graphene	-0.22	Distal	*N$_2$→*N$_2$H	2020[106]
M$_1$M$_2$N$_6$-NG	MoRuN$_6$-NG	-0.17	Enzymatic	*N$_2$→*N$_2$H	2020[107]
M$_2$-phthalocynine (Pc) or MM'-Pc	V$_2$-Pc	-0.39	Mixed (side-on N$_2$ adsorption)	*NH$_2$→*NH$_3$	2020[18]
M$_1$M$_2$-XG (X = C, N, O, P, S)	TiV-CG	-0.30	Enzymatic	*NH$_2$-NH$_3$→ *NH$_3$	2020[108]
TM$_2$@C$_2$N (TM = Sc-Zn, Y-Cd, La-Au)	Cr$_2$@C$_2$N	-0.50	Enzymatic	*N$_2$→*N$_2$H	2020[104c]
Fe$_2$@MoS$_2$	Fe$_2$@MoS$_2$	-0.37	Enzymatic	*N$_2$→*N$_2$H	2020[101]

B$_2$@MoS$_2$	B$_2$@MoS$_2$	-0.19	Enzymatic	*NH$_2$-*NH$_2$→*NH$_2$-*NH$_3$	2019[109]
B, B$_2$@C$_2$N	B$_2$@C$_2$N	-0.35	Enzymatic	*NH$_2$-*NH$_2$→*NH$_2$-*NH$_3$	2019[104b]
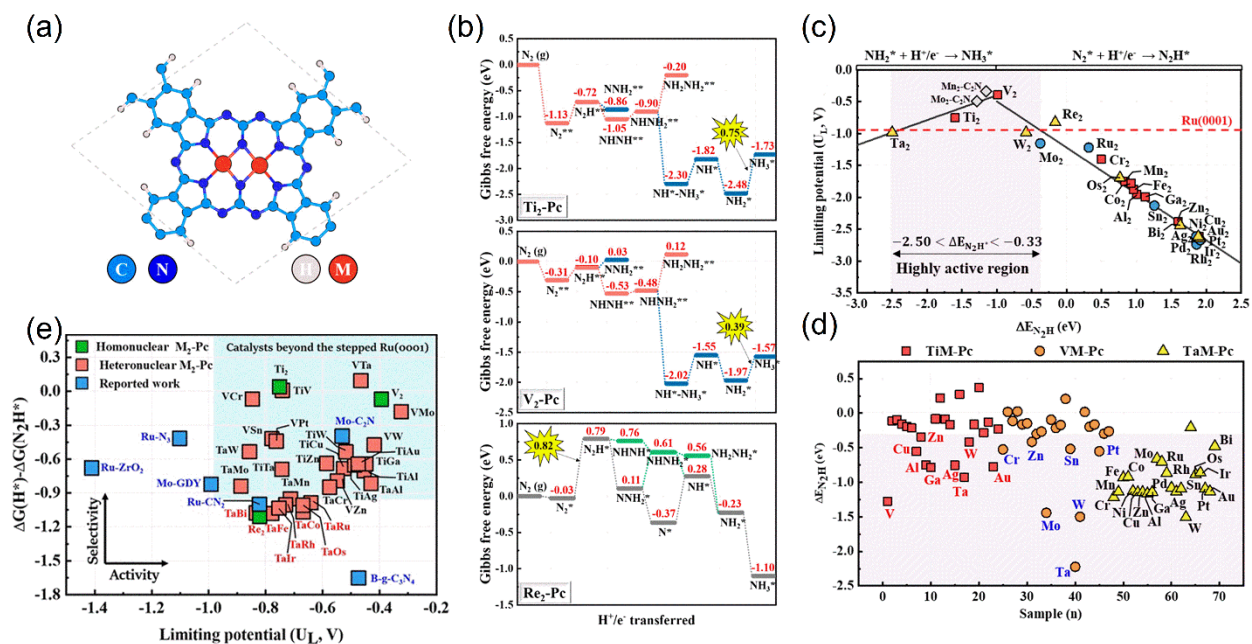
Figure 14. Design of DACs for NRR by theoretical calculations. (a) Structural prototype DACs on 2D Pc nanosheet, (b) Gibbs free energy diagrams for NRR on Ti₂-Pc, V₂-Pc, and Re₂-Pc, (c) volcano plot between NRR limiting potential and adsorption energy of *N₂H, (d) variation of ΔE_{N2H*} on DACs, and (e) $\Delta G(H*)$-$\Delta G(N_2H*)$ versus limiting potential. Reproduced with permission.[18] Copyright 2020, American Chemical Society.

Designing metal-free catalysts instead of TM-based catalysts for NRR is of both environmental and scientific importance.[110] The "acceptance-donation" mechanism has been proposed to describe the adsorption of N_2 on TM-based NRR catalysts: TM atoms with both empty and occupied d orbitals can accept lone-pair electrons from N_2, and donate electrons to the antibonding orbital of N_2 at the same time, leading to the effective activation of N≡N bond and strong adsorption of N_2.[99a, 111] Substituting TM atoms with boron can form metal-free NRR catalysts with comparable activity because boron also possesses both empty and occupied orbitals,

similar to TM atoms.[99a, 111-112] As for DACs, by DFT calculations, Li *et al.* designed dual boron atoms anchored on MoS_2, which showed excellent NRR activity with ultralow overpotential value (0.02 V) and a much lower activation barrier (1.24 eV) compared with those of single boron catalyst B@MoS_2 (0.30 V and 2.84 eV, respectively).[109] Additionally, excellent stability and improved conductivity were also confirmed. Boron dimers on C_2N were also found to possess a lower NRR overpotential (0.19 V) than that of single-atom B@C_2N (0.29 V).[104b] These results suggest that boron dimers instead of single boron atoms could be more promising metal-free DACs for NRR, which appeals for further experimental investigations.

Despite these experimental and theoretical efforts in the design of DACs for NRR, several fundamental issues remain to be addressed. Can a dual-site strategy break the scaling relations for NRR to further enhance the NRR performance? Is there a possibility that new mechanisms be proposed? How does the coordination and ligand effect influence the theoretical NRR activity? All these questions inspire more research into this area.

4.4 CO$_2$RR

CO$_2$ emissions cause the greenhouse effect and global warming; thus, converting CO$_2$ to value-added fuels and chemicals to form a sustainable carbon cycle can offer an enticing opportunity to achieve renewable energy production and mitigate environmental crises simultaneously. For this purpose, electrochemical reduction of CO$_2$ (CO$_2$RR) is among the most appealing techniques because this reaction can occur under ambient conditions.[10, 113] Owing to the stability of the CO$_2$ molecule and the sluggish reaction kinetics, efficient electrocatalysts are in great demand for CO$_2$RR.[114] Conventional metal-based catalysts for CO$_2$RR suffer from

several serious problems, including unsatisfactory overpotential, low selectivity, and high cost, while SACs such as isolated Ni atoms dispersed on carbon materials have been demonstrated as highly efficient active sites for CO_2RR owing to their high AUE and unique electronic properties.[17, 115]

However, some challenging issues for CO_2RR still exist for SACs, such as suppression of the competing reaction HER[116] and scaling relations between the adsorption strength of reaction intermediates (such as *CO, *COOH, *CHO),[41a, 41b, 41d] similar to the case of NRR. In particular, the scaling relations strongly conflict with the common strategy for increasing theoretical CO_2RR performance (increase *CHO binding and weaken *CO binding), thus severely hindering the improvement of the catalytic activity.[41d, 117] Depending on the number of transferred electrons during the CO_2RR, diverse products with different oxidation states of carbon can be generated, which can be categorized into C_1 products, which include CO, formic acid (HCOOH), methanol (CH_3OH), formaldehyde (HCHO), and methane (CH_4), and C_2 products, which include ethanol (C_2H_5OH), ethylene (C_2H_4), and ethanoic acid (CH_3COOH).[114, 118] The complexity of the CO_2RR mechanism, as well as multiple intermediates and products, further limits the catalytic performance of SACs, while the synergistic effect and more sophisticated functionalities in DACs may overcome this limitation, where two atoms in the dimer can provide C-affinity and O-affinity sites to strengthen *COOH or *COH binding without affecting *CO binding so that breaking of scaling relations can occur.[50, 119]

Recently, several groundbreaking experimental studies on DACs for CO_2RR have been reported (**Table 4**). By increasing the Pt mass loading up to 7.5%, Pt dimers on MoS_2 nanosheets were prepared by Li and coworkers.[119a] From the HAADF-STEM image (**Figure 15a**), Pt dimers at neighboring sites were identified, while the atomic dispersion was maintained. The catalytic

performance of the as-obtained DACs revealed that 7.5% Pt/MoS_2 exhibited dramatically enhanced activity compared with that of 0.2% Pt/MoS_2 (Pt SACs) and CO_2 was hydrogenated stepwise to form formic acid and methanol (**Figure 15b**). The TOF for 7.5% Pt/MoS_2 was 162.5 h^{-1}, almost 15 times higher than that for 0.2% Pt/MoS_2 at 150 °C. Further characterization of Pt/MoS_2 by temperature-programmed desorption (TPD) indicated that increasing the Pt loading could lower the H_2 desorption temperature and therefore promote the dissociation of H_2 (**Figure 15c**), and in situ DRIFT results identified two sets of frequencies that belong to COOH* and CH_2OH* intermediates (**Figure 15d**). DFT calculations were performed to investigate the underlying mechanism for Pt SAC and DAC, and HCOOH was found to be more favorable than was $C(OH)_2*$ intermediate on Pt_2/MoS_2, consistent with experimental results (**Figure 15e**). Monolayer MoS_2 offers sites for H_2 dissociation and adsorption of intermediates, which also plays an important role in CO_2RR. In 2019, Jiao *et al.* reported the synthesis of Cu_1^0-Cu_1^{x+} DACs with high selectivity, good activity, and high stability for CO_2RR.[119b] By controlling the Cu loading, different DACs supported on 1D $Pd_{10}Te_3$ nanowires were prepared, and trace amounts of Cu significantly elevated the total current density and therefore activity (**Figure 15f**). The 0.10% Cu sample exhibited enhanced selectivity toward CO in CO_2RR, with the Faradaic efficiency of CO as high as 92% under -0.78 V, and the competing HER was almost completely suppressed (**Figure 15g**). XANES and EXAFS analysis of the valence states and local coordination environment revealed the formation of Cu_1^0-Cu_1^{x+} DACs (**Figure 15h,i**), with Cu_1^{x+} adsorbing H_2O and the paired atom adsorbing CO_2, promoting CO_2 activation. Finally, DFT calculations suggested that Cu-based DACs can reduce the activation energy in CO_2 activation, explaining the excellent catalytic activity of Cu_1^0-Cu_1^{x+} DACs for CO_2RR (**Figure 15j,k**). In another work, cooperative Cu_2^I sites on the Zr_{12} cluster of an MOF (Zr_{12}-bpdc-Cu) were reported.[120] Bimetallic oxidative

addition promotes H_2 activation on Cu centers, and the structures promote C-C coupling to produce methanol in the CO_2RR with >99% selectivity in 10 h.

Table 4. Summary of DACs with the corresponding catalytic activity for CO_2RR.

System	Metal content (wt%)	Main product (Faradaic efficiency)	Current density (mA cm^{-2})	Onset potential (vs. RHE)	Publication year
Pt_2/MoS_2	Pt 7.5	CH_3OH	-	-	2018[119a]
Cu_1^0-Cu_1^{x+}/ $Pd_{10}Te_3$ nanowires	Cu 0.10	CO (92%)	18.74	-0.78 V	2019[119b]
Zr_{12}-bpdc-Cu	-	C_2H_5OH	-	-	2019[120]
Ni/Fe-N-C	Ni 0.97; Fe 0.34	CO (98%)	7.4	-0.7 V	2019[28c]
CoPc/Fe-N-C	Fe 1.04; Co 0.65	CO (93%)	275.6	-0.84 V	2019[121]
AgN_3-AgN_3-graphene	Ag 0.10/0.01 (low loading)	CO (93.4%)	-11.87 (-0.7 V)	-0.25 V	2020[122]
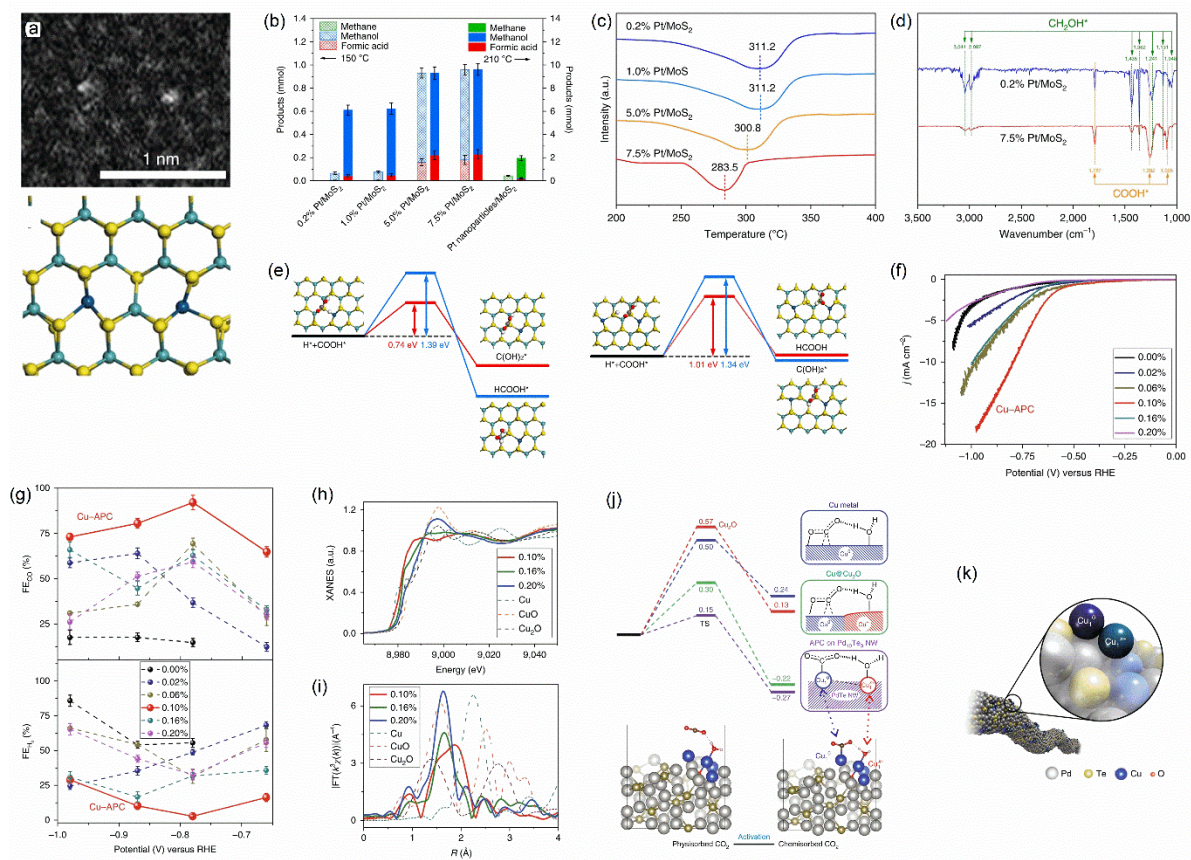
Figure 15. Electrocatalytic performance and characterization of DACs for CO_2RR. (a) HAADF-STEM image of 7.5% Pt/MoS_2, and corresponding structural model, (b) comparison of Pt/MoS_2 with different Pt loading, (c) H_2-TPD profiles, (d) in situ DRIFT spectra of 0.2% and 7.5% Pt/MoS_2 (after exposure to mixed gas $CO_2:H_2 = 1:3$ at 150 °C for 0.5 h), and (e) DFT-identified steps for the addition of H atom to COOH* species on Pt_1/MoS_2 (left) and Pt_2/MoS_2 (right). Reproduced with permission.[119a] Copyright 2018, Nature Publishing Group. (f) Current-voltage curves for different samples from linear sweep voltammetry scans, (g) Faradaic efficiency with different amount of Cu doping at different potentials, Cu K-edge (h) XANES and (i) EXAFS for different samples, (j) free energy profiles for CO_2 activation (top) with the corresponding configurations of CO_2 physisorption and chemisorption (bottom), and (k) illustration of Cu pairs anchored on $Pd_{10}Te_3$ nanowires. Reproduced with permission.[119b] Copyright 2019, Nature Publishing Group.

Like DACs for ORR, metal dimers supported on carbon-based materials have also been reported to exhibit intriguing CO_2RR performance, with the main product being CO. Ren *et al.* designed diatomic Ni-Fe sites anchored on (Ni/Fe-N-C) with a high Faradaic efficiency above 90% for CO over a wide potential range (from -0.5 to -0.9 V) and high durability.[28c] DFT calculations provided theoretical insights that Ni-Fe DACs can decrease the activation barrier for COOH* formation and CO desorption, resulting in a remarkable CO_2RR performance. Lin and coworkers reported the anchoring of cobalt phthalocyanine on Fe-N-C, and the synergistic effect resulted in a significantly broadened 90% Faradaic efficiency window from 0.18 V (Fe-N-C alone) to 0.71 V with an onset potential as low as -0.13 V.[121] Additionally, AgN_3-AgN_3-graphene (Ag_2-G) catalyst was synthesized by binuclear-Ag-based aromatic molecules anchored on graphene, followed by pyrolysis with temperature control.[122] The DACs showed remarkable CO_2RR activity toward CO (93.4% Faradaic efficiency) and high stability, which is far higher than that of Ag SACs. The discovery in this work provides new insights into atomic-scale manipulation of neighboring metal atoms to form DACs and create new paths for understanding heterogeneous catalysis.

In addition to the experimental observations, another group of DACs on 2D materials was predicted by theoretical calculations (**Table 5**). By large-scale DFT calculations and microkinetic modeling, Li *et al.* concluded that multiple homonuclear and heteronuclear dimers on graphene with adjacent vacancies (MM'@2SV) exhibited reduced overpotential and enhanced current density for CO_2RR.[52b] Interestingly, Cu_2, MnCu, and NiCu@2SV can catalyze the CO_2RR and form completely different products: Cu_2@2SV is active toward CO, similar to Au electrodes; MnCu@2SV is selective toward CH_4; and NiCu@2SV is selective toward CH_3OH, which can be attributed to the different oxophilicity between Mn and Ni. The outstanding selectivity, together

with reduced overpotentials, enables the use of DACs as promising catalysts for CO_2RR. In another work, considering that it would be optimal if the two atoms in DACs provide C- and O-affinity sites separately, Ouyang *et al.* designed 21 kinds of heterogeneous TM dimers supported on C_2N and studied their potential CO_2RR applications.[50] (**Figure 16a,b**). By comparing the binding energies of *COOH, *CO, and *CHO, CuCr, CuMn, FeCr, and MnCr dimers were identified with small differences between the binding energies of *CO/*COOH or *CO/*CHO, minimizing the influence of scaling relations (**Figure 16c,d**). The stabilities of the DACs were confirmed by comparing the energy difference between the adsorption energies of the dimers on C_2N and the cohesive energy of metal atoms in their crystals, followed by AIMD simulations. Finally, CuCr and CuMn@C_2N showed the best performance of -0.37 and -0.32 V toward CH_4 production, respectively (**Figure 16e**). Using DFT calculations and microkinetic simulations, Luo and coworkers systematically studied the CO_2RR performance of DACs on N_6-C.[52c] After a two-step screening with *OH and *COOH adsorption free energies, several candidates were excluded because of blocked active sites by *OH or weak *COOH adsorption (**Figure 16f,g**). Finally, CuMn, NiMn, and NiFe DACs were identified to have higher CO_2RR activity toward CO than that of Au(211), the best TM catalyst (**Figure 16h**). These results indicate that DACs supported on 2D materials are promising candidates for breaking the intrinsic scaling relations and improving the CO_2RR activity. However, owing to the complexity of the CO_2RR mechanism and the multifarious reaction products, more experimental and theoretical studies are required.

Table 5. Summary of DFT-predicted DACs for CO_2RR.

System	Best samples	Main product	Theoretical limiting potential (V)	Publication year
TM_2@graphene with adjacent single vacancies (2SV)	Cu_2, MnCu, NiCu@2SV	CO (Cu_2); CH_4 (MnCu); CH_3OH (NiCu)	-0.23 (MnCu); -0.70 (NiCu)	2015[52b]
TM_2@phthalocyanine	Mn_2@phthalocyanine	CH_3OH	-0.84	2017[123]
TM_2@C_2N	Cu_2@C_2N	CH_4 / C_2H_4	-0.23 (CH_4) / -0.76 (C_2H_4)	2018[124]
Ni_2, Co_2, NiCo@C_2N	NiCo@C_2N	CH_4	-0.23	2019[125]
TM_1/TM_2@C_2N	CuCr/CuMn@C_2N	CH_4	-0.37/-0.32	2020[50]
TM_1/TM_2@N_6-C	CuMn, NiMn, NiFe@N_6-C	CO	~ -0.43 (CuMn); ~ -0.45 (NiFe); ~ -0.65 (NiMn)	2020[52c]

Fe$_2$@holey N-doped carbon monolayers	Fe$_2$@C$_2$N	C$_2$H$_5$OH	-0.70	2020[126]
Fe$_n$@graphdiyne (n = 1–4)	Fe$_2$@graphdiyne	CH$_4$	-0.29	2020[127]
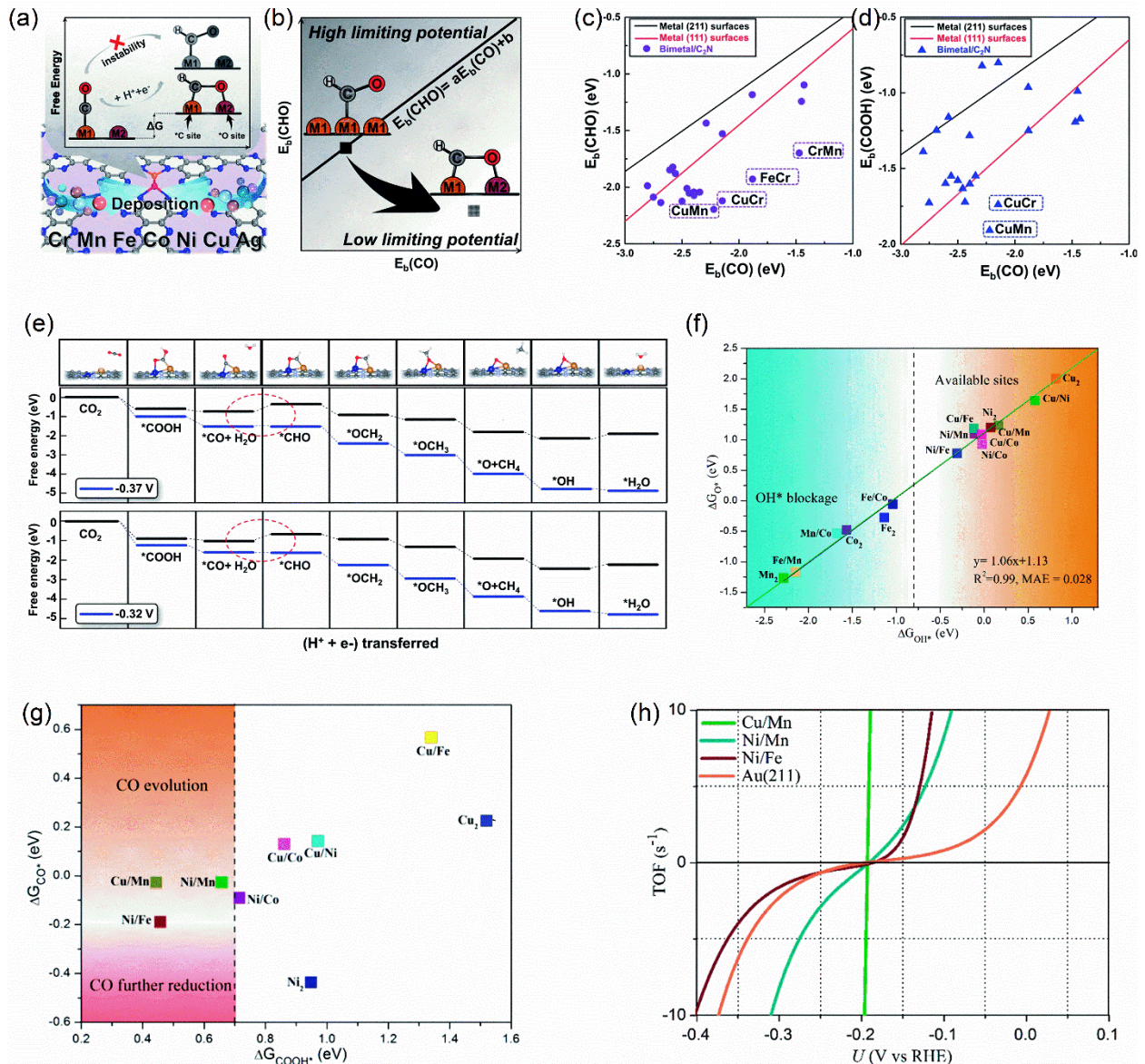
Figure 16. Design of DACs for CO₂RR by theoretical calculations. (a) Design concept of DACs to reduce the free energy change by stabilizing *CHO, (b) schematic of decoupling scaling relations between adsorption energies of *CHO and *CO, and calculated relations between binding energies of (c) *CHO and *CO, (d) *COOH and *CO, (e) CO₂RR free energy diagram toward CH₄ on CuCr/CuMn @C₂N. Reproduced with permission.[50] Copyright 2019, Royal Society of Chemistry. Adsorption free energies of (f) *OH and *O, (g) *COOH and *CO on DACs, (h) TOF for CO₂RR as a function of applied potential for CuMn, NiMn, and NiFe DACs under 0.5 atm, in

comparison with Au(211). Reproduced with permission.[52c] Copyright 2020, Royal Society of Chemistry.

4.5 Other Reactions

In addition to water splitting, ORR, NRR, and CO_2RR, DACs can catalyze a wide range of reactions including CO oxidation reaction (COOR),[88b, 128] hydrolytic dehydrogenation of ammonia borane,[25a] alkaline epoxidation,[27] dry reforming of methane,[129] formic acid dehydrogenation,[130] NO decomposition[131] and oxidation,[132] reverse water–gas shift,[133] HCN production, CO_2 methanation, and alkaline hydrogenation,[134], confirming the broad prospects of DACs.

COOR plays a very important role in reducing the small amount of CO in the environment as well as the hydrogen-rich fuel gases for PEMFCs.[135] SACs for COOR have been intensively studied[136] ever since the concept of single-atom catalysis was introduced by Qiao *et al.* in 2011, who reported high COOR activity of Pt_1/FeO_x SACs.[11] Nevertheless, according to two theoretical observations by Chen's group, DACs can exhibit even higher COOR activity than that of SACs.[88b, 128a] By comparing DACs and SACs through the bi-molecular and tri-molecular Langmuir–Hinshelwood (L-H) and Eley–Rideal (E-R) mechanisms, they came to the conclusion that DAC $Cu_2@C_2N$ possesses better COOR activity than that of its single-atom counterpart $Cu_1@C_2N$.[128a] DFT calculations revealed that O_2 could be more effectively activated on $Cu_2@C_2N$ because of the strong Cu $3d$-O $2p$ orbital hybridization, followed by a low barrier for the first evidence of CO_2 formation at 0.17 eV via the L-H mechanism. On the other hand, the barrier for $Cu_1@C_2N$ was much higher (0.53 eV) via the E-R mechanism. They further extended their studies to

heteronuclear DAC $Fe_1Cu_1@C_2N$, which exhibited better COOR activity than did both $Fe_2@C_2N$ and $Cu_2@C_2N$ without suffering from the CO poisoning problem.[88b] Experimental results also corroborate with theoretical calculations, showing that the synergistic effect in DACs is important for enhancing the COOR activity. Zhou *et al.* synthesized Pt and Ru neighboring monomers anchored on N-vacancy-rich $g-C_3N_4$ by an icing-assisted photocatalytic reduction method.[128b] HAADF-STEM and XAFS confirmed that Pt-Ru dimers in the N_{2C} and C_{2C} sites of the N-vacancy-rich $g-C_3N_4$ indeed exist, and that nitrogen vacancies play an important role in the formation of neighboring monomers. In situ DRIFT spectra and DFT calculations indicated that Pt-Ru dimers are more efficient for optimizing O_2 activation, which is significant in COOR, and can balance the energy evolution of intermediate steps in COOR. These results suggest that DACs exhibit a better catalytic performance for COOR than do SACs owing to the synergistic effect.

5. Conclusions and Future Perspectives

In this review, we summarize the recent progress in the development of DACs, including experimental synthesis (top-down and bottom-up strategies) and characterization methods (TEM and XAFS), theoretical modeling approaches, and practical applications of DACs in energy- and environment-related catalytic reactions (water splitting, ORR, NRR, and CO_2RR). Apparently, double-atom means more than simply doubling the function of a single atom. The synergistic effect from the double-atom provides DACs with the capability of breaking the linear scaling relation, which sheds light on the design of next-generation catalysts. Nevertheless, the applications of DACs are still very limited because of the difficulty in experimental realization, and prospective future research work can be focused on the following issues of DACs:

(1) Precise control of metal dimers in the synthesis of DACs and the application of advanced instrumentation in the characterization of DACs. Compared with SACs, achieving the double-atom nature of DACs is experimentally difficult, appealing for more methodology explorations. ALD has been demonstrated as a potential strategy for the synthesis of both heteronuclear and homonuclear DACs.[25] Recently, Liu *et al.* designed an electrochemical potential window strategy for producing high-purity single-cluster catalysts (SCCs) by theoretical calculations. In the proposed potential window, aggregated metal clusters can be leached away from the substrates and metal single-clusters can be retained owing to strong interactions with the substrates.[137] This method is potentially applicable in the synthesis of DACs, but more experimental evidence is lacking. In addition, other advanced characterization methods can be used to explore the structure–performance relationship of DACs, such as scanning tunneling microscopy, environmental scanning electron microscopy, environmental TEM, and atom probe tomography.

(2) Combining theoretical calculations with experimental observations to conduct a mechanism study. Currently, majority of mechanistic studies of DACs for water splitting, ORR, NRR, and CO_2RR are based on conventional mechanisms. For the mechanism study, one case is the use of noble-metal catalysts for NRR, for which a surface-hydrogenation mechanism was proposed to address the discrepancies between experimental and computational results in the performance that conventional dissociative or associative mechanisms cannot explain.[138] Owing to the synergistic effect between adjacent active sites in DACs, there are possibilities that new mechanisms can better explain the improvement in catalytic performance, which requires further experimental and theoretical investigations.

(3) Prediction of novel DACs using DFT calculations and ML algorithms. Trial-and-error experiments to select potential combinations of metal elements and substrates are infeasible due to high economic cost and time limitations. Instead, the prediction of DACs with theoretical calculations is much more effective. Currently, even though a large number of studies on DFT-predicted high-performance DACs have emerged, most of them are limited to the scale of the data set and cannot provide comprehensive insights for experimental realization. Combining DFT calculations with ML algorithms may be one way to extend the data set to a larger scale, but for DACs, such reports are very scarce, calling for more efforts from theoretical chemists.

Acknowledgements

Conflict of Interest

The authors declare no competing financial interests.

Biographies

Yiran Ying received B.S. in Applied Physics and B.Eng. in Computer Science and Technology (dual degree) from the University of Science and Technology of China in 2016. Currently, he is a

Ph.D. candidate in the Department of Applied Physics, The Hong Kong Polytechnic University, under the supervision of Prof. Haitao Huang. His research interests include computational design of electro/photo-catalysts and 2D materials.
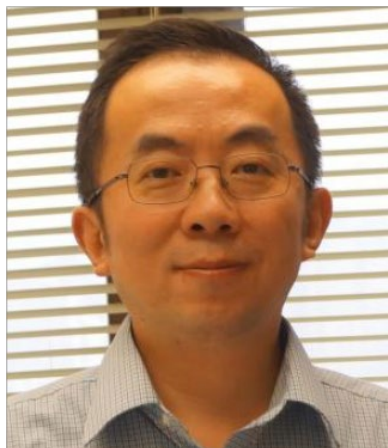
Haitao Huang is a professor in the Department of Applied Physics, The Hong Kong Polytechnic University. His current research interests include electrochemical energy storage and conversion, and ferroelectric materials for energy applications. He is currently the board committee member of the International Academy of Electrochemical Energy Science (IAOEES).

References

[1]   A. S. Arico, P. Bruce, B. Scrosati, J.-M. Tarascon, W. Van Schalkwijk, in *Materials for sustainable energy: a collection of peer-reviewed research and review articles from Nature Publishing Group*, World Scientific **2011**, p. 148.

[2]   B. Dudley, *BP Statistical Review, London, UK* **2019**.

[3]   S. Chu, A. Majumdar, *Nature* **2012**, 488, 294.

[4]   V. R. Stamenkovic, D. Strmcnik, P. P. Lopes, N. M. Markovic, *Nat. Mater.* **2017**, 16, 57.

[5]   Y. Pan, C. Zhang, Z. Liu, C. Chen, Y. Li, *Matter* **2020**, 2, 78.

[6]   a) C. G. Morales-Guio, L. A. Stern, X. Hu, *Chem. Soc. Rev.* **2014**, 43, 6555; b) Y. Jiao, Y. Zheng, M. Jaroniec, S. Z. Qiao, *Chem. Soc. Rev.* **2015**, 44, 2060; c) Y. Zheng, Y. Jiao, M. Jaroniec, S. Z. Qiao, *Angew. Chem., Int. Ed.* **2015**, 54, 52; d) X. Zou, Y. Zhang, *Chem. Soc. Rev.* **2015**, 44, 5148; e) D. Zhao, Z. Zhuang, X. Cao, C. Zhang, Q. Peng, C. Chen, Y. Li, *Chem. Soc. Rev.* **2020**, 49, 2215.

[7]   N. T. Suen, S. F. Hung, Q. Quan, N. Zhang, Y. J. Xu, H. M. Chen, *Chem. Soc. Rev.* **2017**, 46, 337.

[8]   a) Y. Zheng, Y. Jiao, M. Jaroniec, Y. Jin, S. Z. Qiao, *Small* **2012**, 8, 3550; b) L. Dai, Y. Xue, L. Qu, H. J. Choi, J. B. Baek, *Chem. Rev.* **2015**, 115, 4823; c) M. Shao, Q. Chang, J. P. Dodelet, R. Chenitz, *Chem. Rev.* **2016**, 116, 3594; d) M. Liu, L. Wang, K. Zhao, S. Shi, Q. Shao, L. Zhang, X. Sun, Y. Zhao, J. Zhang, *Energy Environ. Sci.* **2019**, 12, 2890.

[9]   a) S. L. Foster, S. I. P. Bakovic, R. D. Duda, S. Maheshwari, R. D. Milton, S. D. Minteer, M. J. Janik, J. N. Renner, L. F. Greenlee, *Nat. Catal.* **2018**, 1, 490; b) X. Cui, C. Tang, Q. Zhang, *Adv. Energy Mater.* **2018**, 8, 1800369; c) C. Guo, J. Ran, A. Vasileff, S.-Z. Qiao, *Energy Environ. Sci.* **2018**, 11, 45.

[10]   a) J. Qiao, Y. Liu, F. Hong, J. Zhang, *Chem. Soc. Rev.* **2014**, 43, 631; b) X. Duan, J. Xu, Z. Wei, J. Ma, S. Guo, S. Wang, H. Liu, S. Dou, *Adv. Mater.* **2017**, 29, 1701784.

[11]   B. Qiao, A. Wang, X. Yang, L. F. Allard, Z. Jiang, Y. Cui, J. Liu, J. Li, T. Zhang, *Nat. Chem.* **2011**, 3, 634.

[12]   a) X.-F. Yang, A. Wang, B. Qiao, J. Li, J. Liu, T. Zhang, *Acc. Chem. Res.* **2013**, 46, 1740; b) J. Liu, *ACS Catal.* **2016**, 7, 34; c) A. Wang, J. Li, T. Zhang, *Nat. Rev. Chem.* **2018**, 2, 65; d) Y. Chen, S. Ji, C. Chen, Q. Peng, D. Wang, Y. Li, *Joule* **2018**, 2, 1242.

[13]   X. Cui, W. Li, P. Ryabchuk, K. Junge, M. Beller, *Nat. Catal.* **2018**, 1, 385.

[14]   a) H. Fei, J. Dong, M. J. Arellano-Jimenez, G. Ye, N. Dong Kim, E. L. Samuel, Z. Peng, Z. Zhu, F. Qin, J. Bao, M. J. Yacaman, P. M. Ajayan, D. Chen, J. M. Tour, *Nat. Commun.* **2015**, 6, 8668; b) H. Fei, J. Dong, Y. Feng, C. S. Allen, C. Wan, B. Volosskiy, M. Li, Z. Zhao, Y. Wang, H. Sun, P. An, W. Chen, Z. Guo, C. Lee, D. Chen, I. Shakir, M. Liu, T. Hu, Y. Li, A. I. Kirkland, X. Duan, Y. Huang, *Nat. Catal.* **2018**, 1, 63; c) Y. Xue, B. Huang, Y. Yi, Y. Guo, Z. Zuo, Y. Li, Z. Jia, H. Liu, Y. Li, *Nat. Commun.* **2018**, 9, 1460.

[15]   a) Y. Chen, S. Ji, Y. Wang, J. Dong, W. Chen, Z. Li, R. Shen, L. Zheng, Z. Zhuang, D. Wang, Y. Li, *Angew. Chem., Int. Ed.* **2017**, 56, 6937; b) H. Zhang, S. Hwang, M. Wang, Z. Feng, S. Karakalos, L. Luo, Z. Qiao, X. Xie, C. Wang, D. Su, Y. Shao, G. Wu, *J. Am. Chem. Soc.* **2017**, 139, 14143.

[16]   a) Z. Geng, Y. Liu, X. Kong, P. Li, K. Li, Z. Liu, J. Du, M. Shu, R. Si, J. Zeng, *Adv. Mater.* **2018**, 30, 1803498; b) L. Han, X. Liu, J. Chen, R. Lin, H. Liu, F. Lu, S. Bak, Z. Liang, S. Zhao, E. Stavitski, J. Luo, R. R. Adzic, H. L. Xin, *Angew. Chem., Int. Ed.* **2019**, 58, 2321.

[17]   H. B. Yang, S.-F. Hung, S. Liu, K. Yuan, S. Miao, L. Zhang, X. Huang, H.-Y. Wang, W. Cai, R. Chen, J. Gao, X. Yang, W. Chen, Y. Huang, H. M. Chen, C. M. Li, T. Zhang, B. Liu, *Nat. Energy* **2018**, 3, 140.

[18]   X. Guo, J. Gu, S. Lin, S. Zhang, Z. Chen, S. Huang, *J. Am. Chem. Soc.* **2020**, 142, 5709.

[19] L. Bai, C. S. Hsu, D. T. L. Alexander, H. M. Chen, X. Hu, *J. Am. Chem. Soc.* **2019**, 141, 14190.

[20] Z. He, K. He, A. W. Robertson, A. I. Kirkland, D. Kim, J. Ihm, E. Yoon, G. D. Lee, J. H. Warner, *Nano Lett.* **2014**, 14, 3766.

[21] P. W. Anderson, *Science* **1972**, 177, 393.

[22] Y. Zhu, J. Sokolowski, X. Song, Y. He, Y. Mei, G. Wu, *Adv. Energy Mater.* **2019**, 10, 1902844.

[23] S. Ji, Y. Chen, X. Wang, Z. Zhang, D. Wang, Y. Li, *Chem. Rev.* **2020**, doi:10.1021/acs.chemrev.9b00818.

[24] J. Lu, J. W. Elam, P. C. Stair, *Acc. Chem. Res.* **2013**, 46, 1806.

[25] a) H. Yan, Y. Lin, H. Wu, W. Zhang, Z. Sun, H. Cheng, W. Liu, C. Wang, J. Li, X. Huang, T. Yao, J. Yang, S. Wei, J. Lu, *Nat. Commun.* **2017**, 8, 1070; b) L. Zhang, R. Si, H. Liu, N. Chen, Q. Wang, K. Adair, Z. Wang, J. Chen, Z. Song, J. Li, M. N. Banis, R. Li, T. K. Sham, M. Gu, L. M. Liu, G. A. Botton, X. Sun, *Nat. Commun.* **2019**, 10, 4936.

[26] a) L. Zhang, J. Fischer, Y. Jia, X. Yan, W. Xu, X. Wang, J. Chen, D. Yang, H. Liu, L. Zhuang, M. Hankel, D. J. Searles, K. Huang, S. Feng, C. L. Brown, X. Yao, *J. Am. Chem. Soc.* **2018**, 140, 10757; b) L. Zhang, Y. Jia, H. Liu, L. Zhuang, X. Yan, C. Lang, X. Wang, D. Yang, K. Huang, S. Feng, X. Yao, *Angew. Chem., Int. Ed.* **2019**, 58, 9404.

[27] S. Tian, Q. Fu, W. Chen, Q. Feng, Z. Chen, J. Zhang, W. C. Cheong, R. Yu, L. Gu, J. Dong, J. Luo, C. Chen, Q. Peng, C. Draxl, D. Wang, Y. Li, *Nat. Commun.* **2018**, 9, 2353.

[28] a) J. Wang, Z. Huang, W. Liu, C. Chang, H. Tang, Z. Li, W. Chen, C. Jia, T. Yao, S. Wei, Y. Wu, Y. Li, *J. Am. Chem. Soc.* **2017**, 139, 17281; b) R. Zhao, Z. Liang, S. Gao, C. Yang, B. Zhu, J. Zhao, C. Qu, R. Zou, Q. Xu, *Angew. Chem., Int. Ed.* **2019**, 58, 1975; c) W. Ren, X. Tan, W. Yang, C. Jia, S. Xu, K. Wang, S. C. Smith, C. Zhao, *Angew. Chem., Int. Ed.* **2019**, 58, 6972; d) W. Ye, S. Chen, Y. Lin, L. Yang, S. Chen, X. Zheng, Z. Qi, C. Wang, R. Long, M. Chen, J. Zhu, P. Gao, L. Song, J. Jiang, Y. Xiong, *Chem* **2019**, 5, 2865.

[29] S. Ji, Y. Chen, Q. Fu, Y. Chen, J. Dong, W. Chen, Z. Li, Y. Wang, L. Gu, W. He, C. Chen, Q. Peng, Y. Huang, X. Duan, D. Wang, C. Draxl, Y. Li, *J. Am. Chem. Soc.* **2017**, 139, 9795.

[30] A. K. Datye, *J. Catal.* **2003**, 216, 144.

[31] C. Kübel, A. Voigt, R. Schoenmakers, M. Otten, D. Su, T.-C. Lee, A. Carlsson, J. Bradley, *Microsc. Microanal.* **2005**, 11, 378.

[32] Y. Zhao, K. R. Yang, Z. Wang, X. Yan, S. Cao, Y. Ye, Q. Dong, X. Zhang, J. E. Thorne, L. Jin, K. L. Materna, A. Trimpalis, H. Bai, S. C. Fakra, X. Zhong, P. Wang, X. Pan, J. Guo, M. Flytzani-Stephanopoulos, G. W. Brudvig, V. S. Batista, D. Wang, *Proc. Natl. Acad. Sci. U. S. A.* **2018**, 115, 2902.

[33] a) A. I. Frenkel, *Chem. Soc. Rev.* **2012**, 41, 8163; b) C. H. van Oversteeg, H. Q. Doan, F. M. de Groot, T. Cuk, *Chem. Soc. Rev.* **2017**, 46, 102.

[34] H. Jin, C. Guo, X. Liu, J. Liu, A. Vasileff, Y. Jiao, Y. Zheng, S. Z. Qiao, *Chem. Rev.* **2018**, 118, 6337.

[35] Z. W. Seh, J. Kibsgaard, C. F. Dickens, I. Chorkendorff, J. K. Norskov, T. F. Jaramillo, *Science* **2017**, 355, eaad4998.

[36] a) P. Hohenberg, W. Kohn, *Phys. Rev.* **1964**, 136, B864; b) W. Kohn, L. J. Sham, *Phys. Rev.* **1965**, 140, A1133.

[37] a) J. K. Norskov, T. Bligaard, J. Rossmeisl, C. H. Christensen, *Nat. Chem.* **2009**, 1, 37; b) A. Kulkarni, S. Siahrostami, A. Patel, J. K. Norskov, *Chem. Rev.* **2018**, 118, 2302.

[38] a) J. K. Nørskov, J. Rossmeisl, A. Logadottir, L. Lindqvist, J. R. Kitchin, T. Bligaard, H. Jonsson, *J. Phys. Chem. B* **2004**, 108, 17886; b) M. Bajdich, M. Garcia-Mota, A. Vojvodic, J. K. Norskov, A. T. Bell, *J. Am. Chem. Soc.* **2013**, 135, 13521; c) J. Zhao, Z. Chen, *J. Am. Chem. Soc.* **2017**, 139, 12480.

[39] D. Friebel, M. W. Louie, M. Bajdich, K. E. Sanwald, Y. Cai, A. M. Wise, M. J. Cheng, D. Sokaras, T. C. Weng, R. Alonso-Mori, R. C. Davis, J. R. Bargar, J. K. Norskov, A. Nilsson, A. T. Bell, *J. Am. Chem. Soc.* **2015**, 137, 1305.

[40]   A. J. Medford, A. Vojvodic, J. S. Hummelshøj, J. Voss, F. Abild-Pedersen, F. Studt, T. Bligaard, A. Nilsson, J. K. Nørskov, *J. Catal.* **2015**, 328, 36.

[41]   a) R. Michalsky, Y.-J. Zhang, A. J. Medford, A. A. Peterson, *J. Phys. Chem. C* **2014**, 118, 13026; b) F. Calle-Vallejo, D. Loffreda, M. T. Koper, P. Sautet, *Nat. Chem.* **2015**, 7, 403; c) J. H. Montoya, C. Tsai, A. Vojvodic, J. K. Nørskov, *ChemSusChem* **2015**, 8, 2180; d) Y. Li, Q. Sun, *Adv. Energy Mater.* **2016**, 6, 1600463.

[42]   V. L. Deringer, A. L. Tchougréeff, R. Dronskowski, *J. Phys. Chem. A* **2011**, 115, 5461.

[43]   J. K. Nørskov, F. Studt, F. Abild-Pedersen, T. Bligaard, *Fundamental concepts in heterogeneous catalysis*, John Wiley & Sons, **2014**.

[44]   Y. Jiao, Y. Zheng, K. Davey, S.-Z. Qiao, *Nat. Energy* **2016**, 1, 16130.

[45]   Y. Liu, J. Wu, K. P. Hackenberg, J. Zhang, Y. M. Wang, Y. Yang, K. Keyshar, J. Gu, T. Ogitsu, R. Vajtai, J. Lou, P. M. Ajayan, Brandon C. Wood, B. I. Yakobson, *Nat. Energy* **2017**, 2, 17127.

[46]   X. Liu, Y. Jiao, Y. Zheng, M. Jaroniec, S. Z. Qiao, *J. Am. Chem. Soc.* **2019**, 141, 9664.

[47]   J. Liu, H. Liu, H. Chen, X. Du, B. Zhang, Z. Hong, S. Sun, W. Wang, *Adv Sci (Weinh)* **2020**, 7, 1901614.

[48]   H. Xu, D. Cheng, D. Cao, X. C. Zeng, *Nat. Catal.* **2018**, 1, 339.

[49]   X. Guo, S. Lin, J. Gu, S. Zhang, Z. Chen, S. Huang, *ACS Catal.* **2019**, 9, 11042.

[50]   Y. Ouyang, L. Shi, X. Bai, Q. Li, J. Wang, *Chem. Sci.* **2020**, 11, 1807.

[51]   a) H. A. Hansen, V. Viswanathan, J. K. Nørskov, *J. Phys. Chem. C* **2014**, 118, 6706; b) M. Besora, F. Maseras, *Wiley Interdiscip. Rev.: Comput. Mol. Sci.* **2018**, 8, e1372.

[52]   a) X. Zhu, J. Yan, M. Gu, T. Liu, Y. Dai, Y. Gu, Y. Li, *J. Phys. Chem. Lett.* **2019**, 10, 7760; b) Y. Li, H. Su, S. H. Chan, Q. Sun, *ACS Catal.* **2015**, 5, 6658; c) G. Luo, Y. Jing, Y. Li, *J. Mater. Chem. A* **2020**, 8, 15809.

[53]   a) G. H. Gu, J. Noh, I. Kim, Y. Jung, *J. Mater. Chem. A* **2019**, 7, 17096; b) A. Chen, X. Zhang, Z. Zhou, *InfoMat* **2020**, 2, 553.

[54]   a) A. D. Sendek, Q. Yang, E. D. Cubuk, K.-A. N. Duerloo, Y. Cui, E. J. Reed, *Energy Environ. Sci.* **2017**, 10, 306; b) A. D. Sendek, E. D. Cubuk, E. R. Antoniuk, G. Cheon, Y. Cui, E. J. Reed, *Chem. Mater.* **2018**, 31, 342.

[55]   J. Im, S. Lee, T.-W. Ko, H. W. Kim, Y. Hyon, H. Chang, *npj Comput. Mater.* **2019**, 5, 37.

[56]   a) K. Tran, Z. W. Ulissi, *Nat. Catal.* **2018**, 1, 696; b) M. Kim, B. C. Yeo, Y. Park, H. M. Lee, S. S. Han, D. Kim, *Chem. Mater.* **2019**, 32, 709; c) M. Sun, A. W. Dougherty, B. Huang, Y. Li, C. H. Yan, *Adv. Energy Mater.* **2020**, 10, 1903949.

[57]   L. Ye, Z. Wen, Z. Li, H. Huang, *Solar RRL* **2020**, 4, 2000027.

[58]   X. Wang, A. Vasileff, Y. Jiao, Y. Zheng, S. Z. Qiao, *Adv. Mater.* **2019**, 31, 1803625.

[59]   D. R. Lide, *CRC handbook of chemistry and physics*, CRC press, **2004**.

[60]   a) J. Zhang, Q. Zhang, X. Feng, *Adv. Mater.* **2019**, 31, 1808167; b) A. Kudo, Y. Miseki, *Chem. Soc. Rev.* **2009**, 38, 253; c) Y. Ying, K. Fan, S. Zhu, X. Luo, H. Huang, *J. Phys. Chem. C* **2020**, 124, 639.

[61]   a) T. Chao, X. Luo, W. Chen, B. Jiang, J. Ge, Y. Lin, G. Wu, X. Wang, Y. Hu, Z. Zhuang, Y. Wu, X. Hong, Y. Li, *Angew. Chem., Int. Ed.* **2017**, 56, 16047; b) Y. Yang, Y. Qian, H. Li, Z. Zhang, Y. Mu, D. Do, B. Zhou, J. Dong, W. Yan, Y. Qin, *Sci. Adv.* **2020**, 6, eaba6586.

[62]   a) Z. Li, H. He, H. Cao, S. Sun, W. Diao, D. Gao, P. Lu, S. Zhang, Z. Guo, M. Li, R. Liu, D. Ren, C. Liu, Y. Zhang, Z. Yang, J. Jiang, G. Zhang, *Appl. Catal., B* **2019**, 240, 112; b) X. Han, X. Ling, D. Yu, D. Xie, L. Li, S. Peng, C. Zhong, N. Zhao, Y. Deng, W. Hu, *Adv. Mater.* **2019**, 31, 1905622; c) X. Zhu, D. Zhang, C.-J. Chen, Q. Zhang, R.-S. Liu, Z. Xia, L. Dai, R. Amal, X. Lu, *Nano Energy* **2020**, 71, 104597.

[63]   X. Zeng, J. Shui, X. Liu, Q. Liu, Y. Li, J. Shang, L. Zheng, R. Yu, *Adv. Energy Mater.* **2018**, 8, 1701345.

[64]   B. Wurster, D. Grumelli, D. Hotger, R. Gutzler, K. Kern, *J. Am. Chem. Soc.* **2016**, 138, 3623.

[65]   Y.-S. Wei, L. Sun, M. Wang, J. Hong, L. Zou, H. Liu, Y. Wang, M. Zhang, Z. Liu, Y. Li, S. Horike, K. Suenaga, Q. Xu, *Angew. Chem. Int. Ed.* **2020**, 59, 16013.

[66]   Y. Zheng, Y. Jiao, Y. Zhu, Q. Cai, A. Vasileff, L. H. Li, Y. Han, Y. Chen, S. Z. Qiao, *J. Am. Chem. Soc.* **2017**, 139, 3336.

[67]   a) Y. Liu, Y. Ying, L. Fei, Y. Liu, Q. Hu, G. Zhang, S. Y. Pang, W. Lu, C. L. Mak, X. Luo, L. Zhou, M. Wei, H. Huang, *J. Am. Chem. Soc.* **2019**, 141, 8136; b) C. Feng, M. B. Faheem, J. Fu, Y. Xiao, C. Li, Y. Li, *ACS Catal.* **2020**, 10, 4019.

[68]   X. Liu, Y. Jiao, Y. Zheng, K. Davey, S.-Z. Qiao, *J. Mater. Chem. A* **2019**, 7, 3648.

[69]   A. Mohajeri, N. L. Dashti, *J. Phys. Chem. C* **2019**, 123, 30972.

[70]   X. Li, S. Duan, E. Sharman, Y. Zhao, L. Yang, Z. Zhuo, P. Cui, J. Jiang, Y. Luo, *J. Mater. Chem. A* **2020**, 8, 10193.

[71]   B. C. Steele, A. Heinzel, in *Materials For Sustainable Energy: A Collection of Peer-Reviewed Research and Review Articles from Nature Publishing Group*, World Scientific **2011**, p. 224.

[72]   D. Higgins, P. Zamani, A. Yu, Z. Chen, *Energy Environ. Sci.* **2016**, 9, 357.

[73]   C. Wan, X. Duan, Y. Huang, *Adv. Energy Mater.* **2020**, 10, 1903815.

[74]   Y. Jiao, Y. Zheng, M. Jaroniec, S. Z. Qiao, *J. Am. Chem. Soc.* **2014**, 136, 4394.

[75]   a) D. Zhang, W. Chen, Z. Li, Y. Chen, L. Zheng, Y. Gong, Q. Li, R. Shen, Y. Han, W. C. Cheong, L. Gu, Y. Li, *Chem. Commun. (Camb)* **2018**, 54, 4274; b) M. Xiao, H. Zhang, Y. Chen, J. Zhu, L. Gao, Z. Jin, J. Ge, Z. Jiang, S. Chen, C. Liu, W. Xing, *Nano Energy* **2018**, 46, 396; c) Z. Lu, B. Wang, Y. Hu, W. Liu, Y. Zhao, R. Yang, Z. Li, J. Luo, B. Chi, Z. Jiang, M. Li, S. Mu, S. Liao, J. Zhang, X. Sun, *Angew. Chem., Int. Ed.* **2019**, 58, 2622; d) G. Zhang, Y. Jia, C. Zhang, X. Xiong, K. Sun, R. Chen, W. Chen, Y. Kuang, L. Zheng, H. Tang, W. Liu, J. Liu, X. Sun, W.-F. Lin, H. Dai, *Energy Environ. Sci.* **2019**, 12, 1317; e) J. Zang, F. Wang, Q. Cheng, G. Wang, L. Ma, C. Chen, L. Yang, Z. Zou, D. Xie, H. Yang, *J. Mater. Chem. A* **2020**, 8, 3686; f) L. Chen, Y. Zhang, L. Dong, W. Yang, X. Liu, L. Long, C. Liu, S. Dong, J. Jia, *J. Mater. Chem. A* **2020**, 8, 4369.

[76]   a) C.-C. Hou, H.-F. Wang, C. Li, Q. Xu, *Energy Environ. Sci.* **2020**, 13, 1658; b) K. Gong, F. Du, Z. Xia, M. Durstock, L. Dai, *Science* **2009**, 323, 760.

[77]   X. Fang, L. Jiao, S. H. Yu, H. L. Jiang, *ChemSusChem* **2017**, 10, 3019.

[78]   J. Wang, W. Liu, G. Luo, Z. Li, C. Zhao, H. Zhang, M. Zhu, Q. Xu, X. Wang, C. Zhao, Y. Qu, Z. Yang, T. Yao, Y. Li, Y. Lin, Y. Wu, Y. Li, *Energy Environ. Sci.* **2018**, 11, 3375.

[79]   M. Xiao, Y. Chen, J. Zhu, H. Zhang, X. Zhao, L. Gao, X. Wang, J. Zhao, J. Ge, Z. Jiang, S. Chen, C. Liu, W. Xing, *J. Am. Chem. Soc.* **2019**, 141, 17763.

[80]   D. Liu, B. Wang, H. Li, S. Huang, M. Liu, J. Wang, Q. Wang, J. Zhang, Y. Zhao, *Nano Energy* **2019**, 58, 277.

[81]   Y. Zhou, W. Yang, W. Utetiwabo, Y. M. Lian, X. Yin, L. Zhou, P. Yu, R. Chen, S. Sun, *J. Phys. Chem. Lett.* **2020**, 11, 1404.

[82]   a) S. Yang, J. Kim, Y. J. Tak, A. Soon, H. Lee, *Angew. Chem. Int. Ed.* **2016**, 55, 2058; b) C. H. Choi, M. Kim, H. C. Kwon, S. J. Cho, S. Yun, H.-T. Kim, K. J. Mayrhofer, H. Kim, M. Choi, *Nat. Commun.* **2016**, 7, 10922.

[83]   C. Tan, X. Cao, X. J. Wu, Q. He, J. Yang, X. Zhang, J. Chen, W. Zhao, S. Han, G. H. Nam, M. Sindoro, H. Zhang, *Chem. Rev.* **2017**, 117, 6225.

[84]   X. Li, W. Zhong, P. Cui, J. Li, J. Jiang, *J. Phys. Chem. Lett.* **2016**, 7, 1750.

[85]   a) E. F. Holby, C. D. Taylor, *Sci Rep* **2015**, 5, 9286; b) Y. Sun, J. Wang, Q. Liu, M. Xia, Y. Tang, F. Gao, Y. Hou, J. Tse, Y. Zhao, *J. Mater. Chem. A* **2019**, 7, 27175; c) Y. Meng, C. Yin, K. Li, H. Tang, Y. Wang, Z. Wu, *ACS Sustain. Chem. Eng.* **2019**, 7, 17273; d) Y. Yang, H. Zhang, Z. Liang, Y. Yin, B. Mei, F. Song, F. Sun, S. Gu, Z. Jiang, Y. Wu, Z. Zhu, *J. Energy Chem.* **2020**, 44, 131.

[86]   a) Z. Liang, M. Luo, M. Chen, C. Liu, S. G. Peera, X. Qi, J. Liu, U. P. Kumar, T. L. T. Liang, *J. Colloid Interface Sci.* **2020**, 568, 54; b) L. Cao, Y. Shao, H. Pan, Z. Lu, *J. Phys. Chem. C* **2020**, 124, 11301−11307.

[87]   X. Zhao, X. Liu, B. Huang, P. Wang, Y. Pei, *J. Mater. Chem. A* **2019**, 7, 24583.

[88]   a) Z. W. Chen, J. M. Yan, Q. Jiang, *Small Methods* **2018**, 3, 1800291; b) F. Li, X. Liu, Z. Chen, *Small Methods* **2019**, 3, 1800480.

[89]   M. A. Hunter, J. M. T. A. Fischer, Q. Yuan, M. Hankel, D. J. Searles, *ACS Catal.* **2019**, 9, 7660.

[90]   a) V. Smil, *Enriching the earth: Fritz Haber, Carl Bosch, and the transformation of world food production*, MIT press, **2004**; b) J. N. Galloway, A. R. Townsend, J. W. Erisman, M. Bekunda, Z. Cai, J. R. Freney, L. A. Martinelli, S. P. Seitzinger, M. A. Sutton, *Science* **2008**, 320, 889.

[91]   C. Zamfirescu, I. Dincer, *J. Power Sources* **2008**, 185, 459.

[92]   D. Bernhardt, J. Reilly II, *US Geological Survey, Reston, USA* **2019**.

[93]   J. Deng, J. A. Iñiguez, C. Liu, *Joule* **2018**, 2, 846.

[94]   C. J. van der Ham, M. T. Koper, D. G. Hetterscheid, *Chem. Soc. Rev.* **2014**, 43, 5183.

[95]   a) S. Wang, F. Ichihara, H. Pang, H. Chen, J. Ye, *Adv. Funct. Mater.* **2018**, 28, 1803309; b) Y. Ying, K. Fan, X. Luo, H. Huang, *J. Mater. Chem. A* **2019**, 7, 11444.

[96]   X. F. Li, Q. K. Li, J. Cheng, L. Liu, Q. Yan, Y. Wu, X. H. Zhang, Z. Y. Wang, Q. Qiu, Y. Luo, *J. Am. Chem. Soc.* **2016**, 138, 8706.

[97]   E. Skúlason, T. Bligaard, S. Gudmundsdóttir, F. Studt, J. Rossmeisl, F. Abild-Pedersen, T. Vegge, H. Jónsson, J. K. Nørskov, *Phys. Chem. Chem. Phys.* **2012**, 14, 1235.

[98]   C. Ling, Y. Ouyang, Q. Li, X. Bai, X. Mao, A. Du, J. Wang, *Small Methods* **2019**, 3, 1800376.

[99]   a) C. Ling, X. Niu, Q. Li, A. Du, J. Wang, *J. Am. Chem. Soc.* **2018**, 140, 14161; b) W. Zhao, L. Zhang, Q. Luo, Z. Hu, W. Zhang, S. Smith, J. Yang, *ACS Catal.* **2019**, 9, 3419; c) B. Huang, N. Li, W.-J. Ong, N. Zhou, *J. Mater. Chem. A* **2019**, 7, 27620; d) F. Liu, L. Song, Y. Liu, F. Zheng, L. Wang, K. Palotás, H. Lin, Y. Li, *J. Mater. Chem. A* **2020**, 8, 3598; e) Y. Ying, K. Fan, X. Luo, J. Qiao, H. Huang, *Mater. Adv.* **2020**, 1, 1285.

[100]   a) N. Cao, Z. Chen, K. Zang, J. Xu, J. Zhong, J. Luo, X. Xu, G. Zheng, *Nat. Commun.* **2019**, 10, 2877; b) Y. Li, Q. Zhang, C. Li, H.-N. Fan, W.-B. Luo, H.-K. Liu, S.-X. Dou, *J. Mater. Chem. A* **2019**, 7, 22242.

[101]   H. Zhang, C. Cui, Z. Luo, *J. Phys. Chem. C* **2020**, 124, 6260.

[102]   a) D. Ma, Z. Zeng, L. Liu, X. Huang, Y. Jia, *J. Phys. Chem. C* **2019**, 123, 19066; b) F. He, Z. Wang, S. Wei, J. Zhao, *Appl. Surf. Sci.* **2020**, 506, 144943.

[103]   Q. Tang, D. E. Jiang, *ChemPhysChem* **2019**, 20, 3141.

[104]   a) X. Zhang, A. Chen, Z. Zhang, Z. Zhou, *J. Mater. Chem. A* **2018**, 6, 18599; b) Y. Cao, S. Deng, Q. Fang, X. Sun, C. Zhao, J. Zheng, Y. Gao, H. Zhuo, Y. Li, Z. Yao, Z. Wei, X. Zhong, G. Zhuang, J. Wang, *Nanotechnology* **2019**, 30, 335403; c) Y. Qian, Y. Liu, Y. Zhao, X. Zhang, G. Yu, *EcoMat* **2020**, 2, e12014.

[105]   W. Yang, H. Huang, X. Ding, Z. Ding, C. Wu, I. D. Gates, Z. Gao, *Electrochim. Acta* **2020**, 335, 135667.

[106]   H. Li, Z. Zhao, Q. Cai, L. Yin, J. Zhao, *J. Mater. Chem. A* **2020**, 8, 4533.

[107]   T. He, A. R. Puente Santiago, A. Du, *J. Catal.* **2020**, 388, 77.

[108]   R. Hu, Y. Li, Q. Zeng, F. Wang, J. Shang, *ChemSusChem* **2020**, 13, 3636.

[109]   F. Li, Q. Tang, *Nanoscale* **2019**, 11, 18769.

[110]   X. Xia, B. Li, S. Liu, B. Tang, *Front Chem* **2020**, 8, 437.

[111]   a) M.-A. Légaré, G. Bélanger-Chabot, R. D. Dewhurst, E. Welz, I. Krummenacher, B. Engels, H. Braunschweig, *Science* **2018**, 359, 896; b) C. Liu, Q. Li, C. Wu, J. Zhang, Y. Jin, D. R. MacFarlane, C. Sun, *J. Am. Chem. Soc.* **2019**, 141, 2884.

[112]   C. Hering-Junghans, *Angew. Chem., Int. Ed.* **2018**, 57, 6738.

[113]   a) M. Aresta, A. Dibenedetto, A. Angelini, *Chem. Rev.* **2014**, 114, 1709; b) L. Ye, Y. Ying, D. Sun, Z. Zhang, L. Fei, Z. Wen, J. Qiao, H. Huang, *Angew. Chem., Int. Ed.* **2020**, 59, 3244.

[114] D. D. Zhu, J. L. Liu, S. Z. Qiao, *Adv. Mater.* **2016**, 28, 3423.

[115] a) X. Li, W. Bi, M. Chen, Y. Sun, H. Ju, W. Yan, J. Zhu, X. Wu, W. Chu, C. Wu, Y. Xie, *J. Am. Chem. Soc.* **2017**, 139, 14889; b) K. Jiang, S. Siahrostami, T. Zheng, Y. Hu, S. Hwang, E. Stavitski, Y. Peng, J. Dynes, M. Gangisetty, D. Su, K. Attenkofer, H. Wang, *Energy Environ. Sci.* **2018**, 11, 893.

[116] Y.-J. Zhang, V. Sethuraman, R. Michalsky, A. A. Peterson, *ACS Catal.* **2014**, 4, 3742.

[117] A. A. Peterson, J. K. Nørskov, *J. Phys. Chem. Lett.* **2012**, 3, 251.

[118] X. Zhu, Y. Li, *Wiley Interdiscip. Rev.: Comput. Mol. Sci.* **2019**, 9, e1416.

[119] a) H. Li, L. Wang, Y. Dai, Z. Pu, Z. Lao, Y. Chen, M. Wang, X. Zheng, J. Zhu, W. Zhang, R. Si, C. Ma, J. Zeng, *Nat. Nanotechnol.* **2018**, 13, 411; b) J. Jiao, R. Lin, S. Liu, W. C. Cheong, C. Zhang, Z. Chen, Y. Pan, J. Tang, K. Wu, S. F. Hung, H. M. Chen, L. Zheng, Q. Lu, X. Yang, B. Xu, H. Xiao, J. Li, D. Wang, Q. Peng, C. Chen, Y. Li, *Nat. Chem.* **2019**, 11, 222.

[120] B. An, Z. Li, Y. Song, J. Zhang, L. Zeng, C. Wang, W. Lin, *Nat. Catal.* **2019**, 2, 709.

[121] L. Lin, H. Li, C. Yan, H. Li, R. Si, M. Li, J. Xiao, G. Wang, X. Bao, *Adv. Mater.* **2019**, 31, 1903470.

[122] Y. Li, C. Chen, R. Cao, Z. Pan, H. He, K. Zhou, *Appl. Catal., B* **2020**, 268, 118747.

[123] H. Shen, Y. Li, Q. Sun, *J. Phys. Chem. C* **2017**, 121, 3963.

[124] J. Zhao, J. Zhao, F. Li, Z. Chen, *J. Phys. Chem. C* **2018**, 122, 19712.

[125] Q. Huang, H. Liu, W. An, Y. Wang, Y. Feng, Y. Men, *ACS Sustain. Chem. Eng.* **2019**, 7, 19113.

[126] Y. Zhao, S. Zhou, J. Zhao, *iScience* **2020**, 23, 101051.

[127] T. He, L. Zhang, G. Kour, A. Du, *J. CO2 Util.* **2020**, 37, 272.

[128] a) F. Li, Z. Chen, *Nanoscale* **2018**, 10, 15696; b) P. Zhou, X. Hou, Y. Chao, W. Yang, W. Zhang, Z. Mu, J. Lai, F. Lv, K. Yang, Y. Liu, J. Li, J. Ma, J. Luo, S. Guo, *Chem Sci* **2019**, 10, 5898.

[129] Y. Tang, Y. Wei, Z. Wang, S. Zhang, Y. Li, L. Nguyen, Y. Li, Y. Zhou, W. Shen, F. F. Tao, P. Hu, *J. Am. Chem. Soc.* **2019**, 141, 7283.

[130] Q. Luo, W. Zhang, C.-F. Fu, J. Yang, *Int. J. Hydrogen Energy* **2018**, 43, 6997.

[131] P. K. Sajith, Y. Shiota, K. Yoshizawa, *ACS Catal.* **2014**, 4, 2075.

[132] Z. Gao, X. Liu, A. Li, X. Li, X. Ding, W. Yang, *Mol. Catal.* **2019**, 470, 56.

[133] H. Chen, Y. Zhang, Q. He, H. Zhang, S. Xu, X. He, H. Ji, *J. Mater. Chem. A* **2020**, 8, 2364.

[134] M. Mon, M. A. Rivero-Crespo, J. Ferrando-Soria, A. Vidal-Moya, M. Boronat, A. Leyva-Perez, A. Corma, J. C. Hernandez-Garrido, M. Lopez-Haro, J. J. Calvino, G. Ragazzon, A. Credi, D. Armentano, E. Pardo, *Angew. Chem., Int. Ed.* **2018**, 57, 6186.

[135] K. Liu, A. Wang, T. Zhang, *ACS Catal.* **2012**, 2, 1165.

[136] a) A. J. Therrien, A. J. Hensley, M. D. Marcinkowski, R. Zhang, F. R. Lucci, B. Coughlin, A. C. Schilling, J.-S. McEwen, E. C. H. Sykes, *Nat. Catal.* **2018**, 1, 192; b) M. J. Hülsey, B. Zhang, Z. Ma, H. Asakura, D. A. Do, W. Chen, T. Tanaka, P. Zhang, Z. Wu, N. Yan, *Nat. Commun.* **2019**, 10, 1330; c) L. Cao, W. Liu, Q. Luo, R. Yin, B. Wang, J. Weissenrieder, M. Soldemo, H. Yan, Y. Lin, Z. Sun, C. Ma, W. Zhang, S. Chen, H. Wang, Q. Guan, T. Yao, S. Wei, J. Yang, J. Lu, *Nature* **2019**, 565, 631.

[137] J.-C. Liu, H. Xiao, J. Li, *J. Am. Chem. Soc.* **2020**, 142, 3375.

[138] C. Ling, Y. Zhang, Q. Li, X. Bai, L. Shi, J. Wang, *J. Am. Chem. Soc.* **2019**, 141, 18264.